

Applied Clay Science

Synthesis of self-cleaning and photoreactive spherical layered double oxide/polymer composite thin layers: biofouling and inactivation of bacteria --Manuscript Draft--

Manuscript Number:	CLAY17683R2
Article Type:	Research Paper
Keywords:	layered double oxide (LDO); composite layers; Superhydrophobicity; photoreactive surfaces; bacterial adhesion
Corresponding Author:	Imre Dékány, DSc. University of Szeged Faculty of Science and Informatics: Szegedi Tudományegyetem Természettudományi és Informatikai Kar Szeged, HUNGARY
First Author:	Imre Dékány, DSc.
Order of Authors:	Imre Dékány, DSc. Ágota Deák, PhD László Janovák Szabolcs Péter Tallósy Karmen Godič-Torkar, PhD Anže Abram Dániel Sebők Klemen Bohinc, DSc
Abstract:	Layered double oxide (LDO) photocatalyst microparticles were synthesized with special radial lamellar orientation. We presented that the 25.31 ± 2.34 nm LDO particles with rough surface can be incorporated in fluoropolymer solution and resulted a composite layer with dual superhydrophobic and photocatalytic properties with high bacterial adhesion and inactivation ability. Next the LDO content in the composite layers were systematically increased (0, 20, 40, 60, 80 and 100 wt.% LDO) which facilitated the surface adhesion of bacteria by electrostatic interactions. The structure of the initial LDO and LDO/fluoropolymer composites was verified by small angle X-ray scattering (SAXS), XRD and SEM measurements. We showed that the surface roughness and hydrophobicity increase with increasing LDO loading. At 80/20 wt.% LDO/fluoropolymer ratio the apparent surface energy was low enough to obtain a superhydrophobic surface ($\theta = 156.3^\circ$ and $\gamma = 2.7$ mJ/m ²). The bacterial adhesion extent on LDO/fluoropolymer composite layers increases with increasing LDO content because the adhesion takes place preferentially to LDO lamellae. The reason for this pronounced adhesion of negatively charged and hydrophilic bacteria onto positively charged and hydrophilic LDO surfaces is the electrostatic attraction between oppositely charged surfaces. The bacterial adhesion was detected by scanning electron and fluorescence microscopy and crystal violet staining assay. Finally, the adhered bacteria were inactivated by the LED-light illumination due to photoreactivity of LDO particles containing 12 wt.% of ZnO phase.
Response to Reviewers:	we would like to thank the Reviewer for his very positive evaluation of our manuscript, and for the insightful comments which truly improved the quality of the manuscript! Please find our detailed answers to the suggestions and comments of the Editor and Reviewer. The modifications are rooted in the comments.

Point-by-point response to the Reviewers' comments

The Reviewers' comments are always followed by our response highlighted in yellow.

Reviewer #1:

First of all, we would like to thank the Reviewer for his very positive evaluation of our manuscript, and for the insightful comments which truly improved the quality of the manuscript!

With respect,

Imre Dékány

Reviewer #1: Manuscript Number: CLAY17683

Reviewer #1: I appreciated the effort made by the authors to modify and integrate the paper following the suggestions received. However, I think that for the article to be published, some changes still need to be made.

In particular, the abstract, in my opinion, is too long, as I had indicated in my previous report. The abstract should concisely include the purpose of the research, the principal results, and conclusions. The abstract contains some information that could be moved to the main text, like, for example, the sentence: "Million of.....oppositely charged surface".

Regarding to the suggestion of the Reviewer#1 the abstract was shortened, see page 1, line 23 – page 2, line 1-22 :

In this paper Layered double oxide (LDO) photocatalyst microparticles were synthesized with special radial lamellar orientation. We presented that the incorporation of 25.31 ± 2.34 μm LDO particles with rough surface into low energy ($\gamma_s^{tot} = 28.0 \text{ mJ/m}^2 \pm 3.91 \text{ mJ/m}^2$) can be incorporated in fluoropolymer solution and resulted a composite layer with dual superhydrophobic and photocatalytic properties with high bacterial adhesion and inactivation ability. The LDO particles with semiconductor properties were prepared by simple calcination of the spherical layered double hydroxide (LDH). Next the LDO content with positive surface charge (+ 0.028 meq/g) in the composite layers were systematically increased (0, 20, 40, 60, 80 and 100 wt.% LDO) which facilitated the surface adhesion of bacteria by electrostatic interactions. The structure of the initial LDO and LDO/fluoropolymer composites was verified by small angle X-ray scattering (SAXS), XRD and SEM measurements. We showed that the surface roughness and hydrophobicity increase with increasing LDO loading. At 80/20 wt.% LDO/fluoropolymer ratio the composite surface roughness was the highest and the apparent surface energy was low enough to obtain a superhydrophobic surface ($\theta_w = 156.3^\circ$ and $\gamma_s^{tot} = 2.7 \text{ mJ/m}^2$). Millions of patients are affected by bacterial infections, which represents a public health risk. The growing bacterial adhesion capacity to different types of surfaces have driven researchers to develop antibacterial and self-cleaning coatings. The bacterial adhesion extent on LDO/fluoropolymer composite layers increases with increasing LDO content because the adhesion takes place preferentially to LDO lamellae. The reason for this pronounced adhesion of negatively charged and hydrophilic bacteria onto positively charged and hydrophilic LDO surfaces is the electrostatic attraction between oppositely charged surfaces. The electrostatic interaction between bacteria and LDO particles was quantitative

determined by surface charge titration. The bacterial adhesion was detected by scanning electron and fluorescence microscopy. The bacterial extent was quantified using and crystal violet staining assay. Finally, the adhered bacteria were inactivated by the LED-light illumination due to photoreactivity of LDO particles containing 12 wt.% of ZnO phase.

Section 2.3, what does "adjusted" mean in the sentence "The nominal (adjusted) LDO/fluoropolymer ratio"?

Thank you for your observation. The "adjusted" is not the correct word to highlighted the prepared ratio of LDO/fluoropolymer. Therefore, we have corrected the sentence to the following (see page 6, line 23):

The nominal LDO/fluoropolymer ratio did not change significantly (0.46–26.8% difference) during the spray-coating film-forming process (Deák et al., 2016).

On page 22, the sentence "The fluorescent dye kit consistswhich cannot penetrate living bacterial cells, only if the cell wall is damaged" is not clear the meaning of the last part of the sentence.

Thank you for your observation. We have corrected the corresponding part to the following (see page 22, line 5):

The fluorescent dye kit consists of two components, SYTO 9 (green) dye and propidium iodide fluorescent dye (PI, red). The SYTO 9 dye enters in both living and damaged bacterial cells, but PI dye cannot penetrate in the living bacterial cells, only if the cell wall is damaged. Although both fluorescent dyes stain the damaged cells, when used together, propidium iodide reduces the intensity of green dye emission (extinguishes) so that only the red color is visible (Tallósy et al., 2016).

In the new fig. 2, the composition of the samples should be indicated above each point of the graph.

Regarding to the suggestion of the Reviewer#1 Fig. 2 was corrected, the composition of the samples was indicated above each point of the graph.

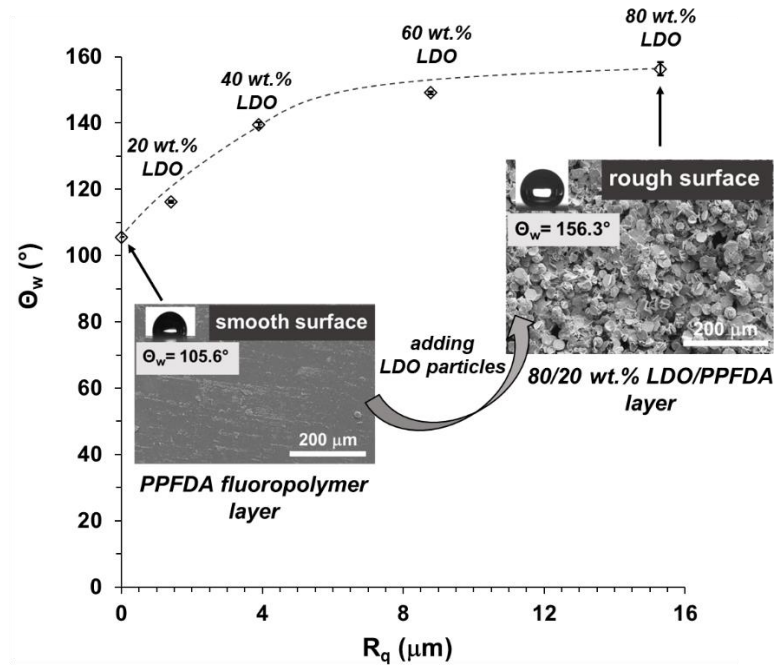


Fig 2. The contact angle values (Θ_w) of composite layers as a function of surface roughness (R_q), ($T = 25 \text{ }^\circ\text{C} \pm 0.5 \text{ }^\circ\text{C}$). Inset: topographies of surfaces with extreme roughness (rough and smooth) with their water contact angle (Θ_w) values and photographs of the liquid droplets on the composite layers. Smooth surface is composed of only fluoropolymer (PPFDA). Rough surface is composed of 80 wt.% LDO and 20 wt.% PPFDA.

English should be revised throughout the text. Occasionally, there are a few typos (initiator, superhydrophobic, etc.).

Thank you for your observation. We have improved the spelling.

[Click here to view linked References](#)

Synthesis of self-cleaning and photoreactive spherical layered double oxide/polymer composite thin layers: biofouling and inactivation of bacteria

Ágota Deák^a, László Janovák^{a,*}, Szabolcs Péter Tallósy^b, Karmen Godič-Torkar^c, Anže Abram^{d,e}, Imre Dékány^a, Dániel Sebők^f, Klemen Bohinc^{c,*}

^aUniversity of Szeged, Department of Physical Chemistry and Materials Science, H-6720, Rerrich Béla tér 1, Szeged, Hungary

^bUniversity of Szeged, Institute of Surgical Research, H-6724, Pulz u. 1, Szeged, Hungary

^cUniversity of Ljubljana, Faculty of Health Sciences, Zdravstvena pot 5, 1000 Ljubljana, Slovenia

^dDepartment for Nanostructured Materials, 'Jožef Stefan' Institute, Jamova cesta 39, 1000 Ljubljana, Slovenia

^eJožef Stefan International Postgraduate School, Jamova cesta 39, 1000 Ljubljana, Slovenia

^fDepartment of Applied and Environmental Chemistry, University of Szeged, H-6720, Rerrich Béla tér 1., Szeged, Hungary

*Corresponding author. Tel.: +36 62 544 209; fax: +36 62 544 042.

E-mail address: janovakl@chem.u-szeged.hu (L. Janovák), klemen.bohinc@zf.uni-lj.si (K. Bohinc)

Abstract

~~In this paper~~ Layered double oxide (LDO) photocatalyst microparticles were synthesized with special radial lamellar orientation. ~~We~~ presented that the ~~incorporation~~ $25.31 \pm 2.34 \mu\text{m}$ LDO particles ~~with~~ rough surface ~~into low energy~~ ($\gamma_s^{\text{tot}} = 28.0 \text{ mJ/m}^2 \pm 3.91 \text{ mJ/m}^2$) ~~can~~ ~~incorporated~~ in fluoropolymer ~~solution~~ and resulted a composite layer with dual

superhydrophobic and photocatalytic properties with high bacterial adhesion and inactivation ability. The LDO particles with semiconductor properties were prepared by simply calcination of the spherical layered double hydroxide (LDH). Next the LDO content with positive surface charge (+0.028 meq/g) in the composite layers were systematically increased (0, 20, 40, 60, 80 and 100 wt.% LDO) which facilitated the surface adhesion of bacteria by electrostatic interactions. The structure of the initial LDO and LDO/fluoropolymer composites was verified by small angle X-ray scattering (SAXS), XRD and SEM measurements. We showed that the surface roughness and hydrophobicity increase with increasing LDO loading. At 80/20 wt.% LDO/fluoropolymer ratio the composite surface roughness was the highest and the apparent surface energy was low enough to obtain a superhydrophobic surface ($\theta_w = 156.3^\circ$ and $\gamma_s^{tot} = 2.7 \text{ mJ/m}^2$). Millions of patients are affected by bacterial infections, which represents a public health risk. The growing bacterial adhesion capacity to different types of surfaces have driven researchers to develop antibacterial and self-cleaning coatings. The bacterial adhesion extent on LDO/fluoropolymer composite layers increases with increasing LDO content because the adhesion takes place preferentially to LDO lamellae. The reason for this pronounced adhesion of negatively charged and hydrophilic bacteria onto positively charged and hydrophilic LDO surfaces is the electrostatic attraction between oppositely charged surfaces. The electrostatic interaction between bacteria and LDO particles was quantitative determined by surface charge titration. The bacterial adhesion was detected by scanning electron and fluorescence microscopy. The bacterial extent was quantified using crystal violet staining assay. Finally, the adhered bacteria were inactivated by the LED-light illumination due to photoreactivity of LDO particles containing 12 wt.% of ZnO phase.

Keywords: layered double oxide (LDO), composite layers, superhydrophobicity, photoreactive surfaces, bacterial adhesion.

1. Introduction

An increasing application of different nano- and microparticles for antimicrobial coatings has been reviewed in the fields of medicine, biology and technology (Zhu et al., 2016; Ghosh et al., 2019). A large part of research related to antimicrobial surfaces was dedicated to hospitals and other health care facilities (Dunne et al., 2018; Chung et al., 2008), where it is demanded that the coated surfaces have well-defined antiseptic and disinfectant properties. Additional self-cleaning properties of newly developed coatings can increase their value and usefulness (Selim et al., 2020; Dunne et al., 2017). Therefore, the study of self-cleaning antimicrobial surfaces has received considerable attention and became an important research topic (Tung et al., 2009; Carja et al., 2009; Sedelnikova et al., 2019; Tung et al., 2011). According to literature, superhydrophobic surfaces with a water contact angle (θ) greater than 150° are one form of self-cleaning surfaces. Walls, paints, textiles, and window glass with self-cleaning property are only a few of the applications for superhydrophobic surfaces (Chen et al., 2016; Saxena et al., 2017; Li et al., 2017; Xue et al., 2017). In general, to achieve superhydrophobic surfaces, the surface roughness should be increased, and the surface energy should be reduced (Liu et al., 2011; Zhang et al., 2017). Increasing the roughness of a hydrophobic solid surface ($\theta > 90^\circ$) could result higher contact angle and superhydrophobic surface ($\theta > 150^\circ$). The conventional superhydrophobic surfaces with antibacterial activity show roughness at both nano- and micro-scale. It is more effective to create water repellent surfaces with roughness scales smaller than 500 nm to prevent potential bacterial trapping and inclusion effects (Hasan et al., 2015; Nosonovsky et al., 2009).

The photocatalytic coatings are another group of self-cleaning surfaces, which is able to decompose various organic materials under light exposure (Li et al., 2020; Fresno et al., 2014). Semiconductor particles (*e.g.* TiO_2 or ZnO) show photocatalytic activity (Fateh et al., 2014) and produce highly reactive oxygen species like superoxide radical ion (O_2^-), hydrogen peroxide (H_2O_2), or hydroxyl radical (HO^\cdot) (Fujishima and Honda, 1972) under light

exposure. These reactive species are able to inactivate both organic compounds and the microorganisms (Veres et al., 2012; Tallósy et al., 2014).

Bacterial adhesion to different surfaces is a complex phenomenon that is influenced by the physical and chemical characteristics of the surfaces as well as the bacterial cells themselves (Bayoudh et al., 2008; Xie et al., 2018). Surface properties such as surface roughness, charge, and degree of hydrophobicity influence the intensity of bacterial adhesion (Bos et al., 1999; Bohinc et al., 2014, 2016). Beside the surface properties, the intensity of bacterial adhesion is also influenced by the charge of the bacterial cell wall, hydrophobicity, flagellation and motility (Bos et al., 1999). Environmental factors (e.g. temperature, pH, nutrient composition, etc.) enhance the bacterial adhesion and the growth of biofilms (Herrald and Zootolla, 1988; Raghunath and Perumal, 2017).

In our previous work (Deák et al., 2016) we have presented the synthesis and advantage of inorganic/organic hybrid layers with dual superhydrophobic and photoreactive properties. These superhydrophobic layers were synthesized using ~25 μm layered double oxide (LDO) photocatalyst particles and low surface energy poly(perfluorodecyl acrylate) (PPFDA) fluoropolymer binder material. The application of PPFDA resulted a decrease in the surface free energy of the hydrophilic LDO. The structured surface LDO photocatalyst particles with ~12% nominal ZnO content (Deák et al., 2016) were synthesized from layer double hydroxide (LDH) spheres. The morphological characteristics of LDH are significantly affected by the synthesis conditions: at alkaline pH values ($\text{pH} > 8$) lamellar LDH is formed, whereas at acidic pH values ($\text{pH} = 3$), in the presence of urea, spherical LDH can be obtained (Deák et al. 2015). The determined excitation wavelength and the calculated band gap energy values were 386 nm and 3.23 eV, respectively. It was found that the simultaneous superhydrophobic behaviour ($\Theta > 150^\circ$) and the satisfactory photocatalytic properties of the thin film occurred at 80-90 wt% LDO content. The determined surface free energy value of the superhydrophobic hybrid layer with 80 wt% LDO content was 11.8 mJ/m². In the benzoic acid photodegradation

test experiments, the hybrid layers with 80-90 wt% LDO content photodegraded 22-24% of the initial test molecule concentration (0.17 g/L) under UV-A ($\lambda_{\text{max}} = 365 \text{ nm}$) illumination. Thus, based on these results, the main goal of the present work is to study the bacterial adhesion and photocatalytic inactivation ability on these composite. The bacterial adhesion extent was investigated using the crystal violet staining assay. The LDO lamellae surface with adhered bacteria was examined using scanning electron microscopy micrographs. With adjusting the loading of spherical LDO particles into composite layers the surface roughness, the surface charge density, the wetting properties and thus the bacterial adhesion capacity are controlled. The surface roughness was investigated by profilometric measurements and the surface charge was determined with the manual titration using a Particle Charge Detector. Water contact angle measurements were used to estimate the hydrophobicity of the composite layers. To inactivate the adhered bacteria the photoreactive LDO/fluoropolymer composite surface was illuminated by LED-light and the photoreactivity was also evidenced by luminometric measurements. Fluorescence microscopy measurements were used to detect live and dead bacteria on the composite layer.

2. Materials and methods

2.1. Preparation of LDO particles

The layered double oxide (LDO) was prepared by calcination process of the spherical layered double hydroxide (LDH) (Deák et al., 2016). LDH was synthesised by a simply co-precipitation method using magnesium nitrate hexahydrate ($\text{Mg}(\text{NO}_3)_2 \cdot 6\text{H}_2\text{O}$, 98%; Sigma-Aldrich, United Kingdom), zinc nitrate hexahydrate ($\text{Zn}(\text{NO}_3)_2 \cdot 6\text{H}_2\text{O}$, 99%; Fluka Chemika, Croatia), and aluminium nitrate nonahydrate ($\text{Al}(\text{NO}_3)_3 \cdot 9\text{H}_2\text{O}$, 99,7%; Molar Chemicals KFT, Hungary) as precursors. The molar ratio of $(\text{Zn} + \text{Mg}):\text{Al}$ was 2:1 and the $\text{Zn}:\text{Mg}$ was 1:8. During the process, urea $((\text{NH}_2)_2\text{CO}$, 98%, Sigma-Aldrich, Germany) was used as a gas bubble forming agent. The resulting precipitate was aged at 98 °C, then centrifuged, washed

with distilled water, and dried in a 60 °C oven (overnight). The resulted LDH powder was calcinated 2 hours at 600 °C to obtain LDO particles. The XRD patterns presents the formation of oxide phase for LDO see in *Supporting Information*, Fig. S1.

2.2. Synthesis of fluoropolymer binder

1H, 1H, 2H, 2H-perfluorodecyl acrylate (PFDA) monomer and 2-dimethoxy-2-phenylacetophenone (Irgacure 651) initiator were used for the synthesis of fluoropolymer. The **initiator** and monomer were obtained from Aldrich Chemical and were used without further purification. The fluoropolymer sample of poly(1H, 1H, 2H, 2H-perfluorodecyl acrylate) (PPFDA) was dissolved in butyl-acetate (10 wt.% polymer solution) and used to produce composite layers. Molecular weight determination of synthesized fluoropolymer was performed by using dynamic light scattering (DLS) measurements. The weight average (M_w) molecular weight of the obtained PPFDA was 56 kDa (see in *Supporting Information*, Fig. S2).

2.3. Preparation of LDO/fluoropolymer composites

The LDO containing composite layers were prepared on 5×5 cm² glass plates using a gravity feed airbrush (ChroMax BD-203) sprayer gun with 3 bar operating pressure. The loading of the LDO particles in the composite layers were 0, 20, 40, 60, 80 and 100 wt.%, respectively inserted into the low energy fluoropolymer binding material. 10 wt% aqueous suspensions were prepared with varied LDO/fluoropolymer content. The gravimetrically measured specific amount of material deposited on the glass plates was 5.8 ± 0.1 mg/cm² in each case.

The nominal LDO/fluoropolymer ratio did not change significantly (0.46–26.8% difference) during the spray-coating film-forming process (Deák et al., 2016).

2.4. Structural and surface information of the LDO/fluoropolymer composite layers – SAXS measurements

Small-angle X-ray Scattering (SAXS) curves were recorded with a slit-collimated Kratky compact small-angle system (KCEC/3 Anton-Paar KG, Graz, Austria) to obtain structural and surface information about the LDO/fluoropolymer composites. The used calculations were include in the *Supporting Information*.

2.5. Surface morphology and elemental composition – scanning electron microscopy (SEM)

The structure and the morphology of the synthesized hydrophilic LDO particles and LDO/fluoropolymer composite layers were examined by field emission scanning electron microscopy (SEM – Hitachi S-4700 microscope), applying a secondary electron detector and 10 kV acceleration voltage. Röntec EDX detector was used for elemental distribution of Al and F atoms for LDO and PPFDA polymer materials in the LDO/fluoropolymer composite layers.

The surface shape and distribution of microorganisms adhered to the composite layers were imaged using a scanning electron microscope (Jeol FEG-SEM 7600F).

2.6. Surface roughness

A mechanical profilometer was used to examine the surface roughness of the LDO/fluoropolymer composite layers (Form Talysurf Series 2 from Taylor Hobson Ltd., Leicester, Great Britain). Roughness and waviness were separated using a 0.25 mm Gaussian cut-off filter. The applied length scale was 2000 μm because this scale is long enough to get appropriate average roughness value about the composites with surface microstructure and roughness.

2.7. Apparent static and dynamic contact angle measurements

The hydrophobicity of the composite layers was determined by water contact angle (θ_w). We used an EasyDrop drop shape analysis device (Krüss GmbH, Hamburg, Germany) with a Peltier temperature chamber and a 0.5 mm diameter syringe steel needle. The tests were carried out at room temperature and under normal atmospheric conditions.

Drelich's protocol was used to calculate the advancing (θ_{adv}) and receding (θ_{rec}) contact angles (Drelich et al., 2013). From the obtained angles the total apparent surface free energy (γ_s^{tot}) of the layers was calculated. Knowing the surface tension of distilled water ($\gamma_1 = 72.1$ mN/m at 25 °C) and its contact angle hysteresis defined as the difference between the advancing and receding contact angles (Chibowski et al., 2003) we calculate γ_s^{tot} :

$$\gamma_s^{tot} = \left(\frac{\gamma_1(1+\cos \theta_{adv})^2}{(2+\cos \theta_{rec}+\cos \theta_{adv})} \right) \quad (1)$$

Contact angle measurements were also used to evaluate the polar and dispersive elements. Overall surface free energy (γ_s^{tot}) and its polar (γ_s^P) and dispersion (γ_s^D) components of the composites with increasing LDO loading were determined from two sets of contact angles (water and glycerin) according to Owens-Wendt-Kaelble equation (Owens and Wendt, 1969).

$$\gamma_1(1 + \cos \theta) = 2[\gamma_1^D \gamma_s^D]^{1/2} + 2[\gamma_1^P \gamma_s^P]^{1/2} \quad (2)$$

where, γ_1 is the surface free energy of the liquid; θ is the contact angle of a liquid against the solid. The dispersion component of the surface free energy for liquid is γ_1^D and for solid is γ_s^D . For a liquid, the polar portion of the surface free energy is γ_1^P , whereas for a solid, it is γ_s^P . The obtained surface free energies values of the test liquids from the literature are given in Fig. S3 as inserted table (Torchinsky and Rosenman, 2009).

The underwater stability of the composite layer with 80 wt.% LDO loading was also determined. During the process the composite layers were submerged under the water for 24 hours. Then, the layers were taken out from the water after different immersion time and the wetting properties were characterized by the sessile drop contact angle (θ_w) measurement. At the end of the experiment the composite layers were re-dried and the contact angle were re-measured.

2.8. Preparation of the bacterial cultures

We used three different standard bacterial strains: *Escherichia coli* (*E. coli*) ATCC 35218, *Pseudomonas aeruginosa* (*P. aeruginosa*) ATCC 27853 and *Staphylococcus aureus* (*S. aureus*) ATCC 25923. The three different strains of bacteria were transferred on nutrient agar and incubated at 37 °C 24 h. To obtain the overnight culture, a single colony of each strain was transferred from nutrient agar to nutrient broth (Biolife, Italy) and incubated at the same conditions.

2.9. Surface charge measurements

Surface charge of LDO photocatalyst was measured by PCD-04 Particle Charge Detector (Mütek Analytic GmbH, Germany) with manual titration. During the process 10 mL of 1 wt.% LDO suspension was titrated with 0.1 wt.% sodium dodecyl sulphate (SDS) negatively charged surfactant solution. Then, 10 mL of 1 wt.% LDO suspension was titrated with 10⁵ CFU/mL *E. coli* bacterial suspension at the same experimental condition like in the bacterial adhesion measurements.

The equimolar amount of surfactant or bacteria CFU was determined to the amount of LDO (meq/g or CFU/g), taking into consideration the amount of the added surfactant or bacteria (at the charge neutralization point where the streaming potential equal to 0 mV).

2.10. Monitoring the bacterial adhesion extent

The method of Bohinc et al. (Bohinc et al., 2014) with modifications was used as follows. 1.33 mL of bacterial overnight cultures ($10^8 - 10^9$ CFU/mL) were transferred into 40 mL of fresh nutrient broth, to obtain the concentration from $10^7 - 10^8$ CFU/mL. The sterile LDO/fluoropolymer composite layer coupons (1 cm \times 1 cm) were placed into the Petri dishes and 20 mL of the diluted bacterial culture was added. For negative control we used 20 mL of fresh nutrient broth without bacterial culture for each type of coupons.

The bacterial cells adhered to the composite surfaces immediately after inserting the coupons horizontally in the broth (time 0) and after an 18-hour incubation period at 37 °C in aerobic conditions without shaking. The nutrient broth with bacterial culture was removed after the incubation time. The coupons were rinsed five times with sterile PBS buffer before being stained for 5 minutes at room temperature with 3 mL 0.1 percent (w/v) crystal violet suspension (Merck, Germany). PBS buffer was used to wash the system five times more. The dye was remobilized from the cells with 400 μ L 96 % ethanol for three minutes. The optical density of the extracted dye was measured at wavelength 620 nm (OD_{620}) by microplate reader Infinite 200[®] PRO, Tecan Austria GmbH.

The number of adhered bacterial cells was investigated with scanning electron microscope (Jeol FEG-SEM 7600F). The adhered bacterial cells on the surfaces were expressed as bacterial cells /cm² determined from several SEM micrographs (Kovačević et al., 2016).

2.11. Fluorescence measurements

P. aeruginosa ATCC 27853 was detected by the fluorescence measurements (Tallósy et al., 2016). During the fluorescence experiments 6 μ L of the dye mixture was added for each mL of bacterial suspension ($1 \times 10^5 - 5 \times 10^5$ CFU/mL). In a two-component formulation, the fluorescence dye was used. Component I (SYTO 9) is able to penetrate the bacterial cell wall and mark the DNA of both living and dead bacteria. Component II (Propidium iodide: PI) is

incapable of penetrating a bacterial cell wall which is still intact. It can penetrate only in bacteria with damaged membranes, causing a reduction in the SYTO 9 stain fluorescence. According to the user's guide of the viability kit (LIVE/DEAD® BacLight™ Bacterial Viability kit L7007, Life Technologies, Hungary), the bacteria were grown in nutrient broth (Mueller-Hinton) to late logarithmic phase, then placed on the composite surfaces and exposed to blue LED-light (General Electric's, Hungary, $\lambda_{\text{max}} = 405 \text{ nm}$) for 0, 60, and 120 minutes.

The viability of the bacteria was evaluated with fluorescence microscope (Leica DM IL LED Fluo). Fluorescence at exc./emi. maxima of about 480/500 nm for SYTO 9 stain (green) and 490/635 nm for PI was used to quantify the reduction of live bacteria after different illumination times of the composite layers (red). Thus, intensities of the green and red emission caused by the live and dead bacteria were recorded. The ratio between the number of red and green coloured bacterial cells on the surface was determined after illumination of LED-light.

2.12. The formation of hydroxyl radicals on LDO/fluoropolymer composite layers

The number of reactive hydroxyl radicals at the solid/liquid interface was calculated using the hydrogen peroxide driven luminol based chemiluminescence reaction (Tallósy et al., 2014a, 2014b, 2016). Results were calculated from the chemiluminescence (CL) data obtained from SiriusL Single Tube luminometer (Berthold Detection Systems, Budapest). According to the measurement protocol 3 mg luminol (Sigma-Aldrich) was diluted in 0.5 mL of sodium hydroxide (0.1 M) and filled out to 10 mL with distilled water. The composite layers (5 cm × 5 cm) were immersed in 40 mL distilled water and illuminated with LED-light ($\lambda_{\text{max}} = 405 \text{ nm}$) and continuously shaken. The distance of the LED-light source from the composite films was 5 cm. Then, 100 μL samples were taken after 2.5, 5, 10, 15, 20, 30, 40, 50, 60, 75 and 90 minutes of illumination time and were added to 100 μL of luminol solution of concentration

33.8 mM. The intensity of the CL was measured immediately by the luminometer. The calibration curve was previously determined in the range of 0 - 5 mM of hydrogen peroxide (Fig. S4). The calculated concentration of ROS (expressed as $C_{H_2O_2}$ equivalent) coming from the decomposition of H_2O_2 is directly proportional to the measured relative light unit (RLU/s):

$$C_{H_2O_2} = \frac{(RLU/s)}{41866} \quad (2)$$

where 41866 is the slope of the calibration curve.

From the RLU data, the free radical concentration was computed using $C_{H_2O_2}$ and plotted as a function of illumination time for varying LDO concentrations within the layer.

2.13. Mechanical stability measurements

To evaluate the abrasion resistance of coatings the taber abraser test is frequently used (Rossi et al., 2009). A 418 type manual Taber Abraser was used for the abrasion tests. During the measurement the composite sample with 80 wt.% LDO content was abraded and the contact angles of the tested surfaces were measured as a function of abrasion cycle.

3. Results and discussion

The purpose of our study was to obtain antibacterial and water-repellent coatings, which have low surface free energy and rough surface structures. This can be obtained with LDO particles embedded into the low energy PPFDA fluoropolymer matrix. We measured the structural, morphological, photocatalytic and bacterial adhesion properties of these composite layers.

3.1. Surface roughness and contact angle determination of the composite layers

The morphological characteristics of LDH are significantly affected by the synthesis conditions. In the presence of urea, spherical LDH can be obtained (Deák et al., 2015). One

possible explanation for the formation of spherical LDH is that in a medium containing carbonates, at low pH (pH= 3) and high temperature, the decomposition of urea gives rise to NH_3 and CO_2 gas bubbles, initiating nucleus formation.

After a calcination method, the original Zn content of the special ZnMgAl-LDH (Deák et al., 2016) was converted into photocatalytically active ZnO content layered double oxide (LDO). The ZnO content of LDO was calculated from the Zn content of the initial LDH assuming complete oxidation during the calcination. The original spherical morphology of LDH was still retained and $25.31 \pm 2.34 \mu\text{m}$ spherical LDO particles were obtained (Fig. 1).

Fig. 2 shows the contact angle values of composite layers as a function of surface roughness (R_q). As it can be seen the increase of the LDO content (from 20 wt.% to 80 wt.%) resulted and increase in the R_q values from $0.002 \mu\text{m} \pm 0.0002 \mu\text{m}$ to $15.3 \mu\text{m} \pm 2.04 \mu\text{m}$ and consequently the Θ_w values were also increased from 105.6° to 156.3° . The inset of Fig. 2 shows SEM micrographs of the smooth and rough surfaces. Increasing the LDO content in the composite layers resulted greater surface roughness and contact angle values. 149.1° and 156.3° contact angles were achieved at 60 and 80 wt.% LDO content. This indicates that the superhydrophobic layers were obtained. Due to the hydrophilic characteristic of LDO particles, a pure LDO layer (without fluoropolymer coating) is superhydrophilic and we were able to achieve a fine, superhydrophilic surface in this manner.

Furthermore, the obtained thickness of the layers were between $64 \pm 1.03 \mu\text{m}$ and $197 \pm 1.80 \mu\text{m}$ (see Fig. S5). The thickness and porosity increases with the increasing LDO content which is also clearly visible from the presented SEM micrographs (Fig. S6). The porosity of films varies between 17.5 and 58.1% (Deák et al., 2016).

The EDX measurements also reveal that the surface of the composite is uniform and the elemental distribution of the Al from LDO and F from PPFDA is in accordance with the LDO loading (Fig. S7).

We consider the mechanical durability of the composite coating because the water repellent superhydrophobic surfaces are highly susceptible to abrasion damage during the service. The angle θ decreases with the aggravated abrasion and it takes a constant value of $\sim 136^\circ$ after 20 cycles (Fig. 3). Even though the coating has lost its superhydrophobicity, the inserted EDX pictures show that the above presented heterogeneous surface structure with simultaneous presence of LDO and fluoropolymer doesn't change.

3.2. Surface energy of LDO/fluoropolymer composite

The surface hydrophobicity of composite layers was characterized by the dynamic contact angle measurement determining the advancing (θ_{adv}) and receding (θ_{rec}) contact angles (Fig. 4). With increasing volume of the water droplet on the pure PPFDA fluoropolymer layer the advancing contact angle (θ_{adv}) decreases from $\theta_{(6.1\mu l)} = 105.6^\circ$ to $\theta_{(49.7\mu l)} = 89.1^\circ$ (Fig. 4). The receding contact angle (θ_{rec}) is progressively decreasing with decreasing volume of the droplet and the final value is significantly lower ($\theta = 24.7^\circ$) than the static contact angle (105.6°). This high contact angle hysteresis ($\Delta\theta_w = 80.9^\circ$) indicates a relatively good wetting properties of the pure fluoropolymer layer. However, in the case of rough superhydrophobic composite layer with 80 wt.% of LDO content, the Θ_{adv} was changed from $\theta_{(7.0\mu l)} = 156.1^\circ$ to $\theta_{(44.6\mu l)} = 150.2^\circ$. The Θ_{rec} changed for smaller amount from 150.2° to 143.7° . The angle hysteresis was $\Delta\theta_w = 12.4^\circ$ which is characteristic for superhydrophobic surfaces (McHale et al., 2004). The total apparent surface free energy γ_s^{tot} calculated from Equation (1) is $28.0 \text{ mJ/m}^2 \pm 3.91 \text{ mJ/m}^2$ for pure polymer whereas for the superhydrophobic composite layer $\gamma_s^{tot} = 2.7 \text{ mJ/m}^2 \pm 0.65 \text{ mJ/m}^2$.

The surface energy demonstrates the differences between the two types of surfaces. The PPFDA polymer with a low surface free energy $\gamma_s^{tot} = 28.0 \text{ mJ/m}^2 \pm 3.91 \text{ mJ/m}^2$ with smooth surface ($R_q = 0.002 \mu\text{m} \pm 0.0002 \mu\text{m}$) was further reduced to $\gamma_s^{tot} = 2.7 \text{ mJ/m}^2 \pm 0.65 \text{ mJ/m}^2$ with the enhanced surface roughness ($R_q = 15.3 \mu\text{m} \pm 2.04 \mu\text{m}$) of the composite layer

containing 80 wt.% of LDO. Thus, after the roughening process the hydrophobic layer showed superhydrophobic properties. This reducing tendency of the surface free energy caused by the increasing roughness is presented in Fig. S8. The increased ratio of incorporated LDO particles in the fluoropolymer from 0 to 80 wt.% caused a continuous increase of R_q from $0.002 \mu\text{m} \pm 0.0002 \mu\text{m}$ to $15.3 \mu\text{m} \pm 2.04 \mu\text{m}$ and continuous decrease of γ_s^{tot} from $28.0 \text{ mJ/m}^2 \pm 3.91 \text{ mJ/m}^2$ to $2.7 \text{ mJ/m}^2 \pm 0.65 \text{ mJ/m}^2$.

The total surface free energy (γ_s^{tot}) and its polar (γ_s^P) and dispersion (γ_s^D) components were also determined in accordance with to Owens-Wendt-Kaelble equation (see Fig. S3). Since PPFDA is a chemically inert and hydrophobic fluoropolymer, it has a relatively low γ_s^{tot} ($24.65 \pm 0.56 \text{ mJ/m}^2$) mainly with γ_s^P contribution. Increasing the LDO loading, the γ_s^{tot} values were continuously decreased to $3.39 \pm 0.68 \text{ mJ/m}^2$ (80 wt.% LDO content). Over 80 wt.% LDO loading, the γ_s^{tot} was drastically increased ($62.40 \pm 0.98 \text{ mJ/m}^2$ at 100% LDO content) and the ratio of γ_s^P and γ_s^D values was also changed ($13.77 \pm 0.93 \text{ mJ/m}^2$ and $48.63 \pm 1.04 \text{ mJ/m}^2$) indicating the hydrophilic surface characteristic of the film. This is because over 80% LDO content the surface is mainly covered by hydrophilic LDO (see EDX results in Fig. S7) and the surface turns from hydrophobic to hydrophilic.

3.3. SAXS measurements

The micro surface roughness of the layers was presented in Fig. 2, however, the composite layers also have nanostructural arrangements and inner surface morphology. SAXS scattering curves (Fig. S9) was used to determine the surface roughness and the specific surface area of the LDO/fluoropolymer composite layers on nanoscale.

The $\ln(h^3I)$ vs. h^2 (Porod) plot of the SAXS scattering curves (Fig. S9) was used to determined the surface roughness and the specific surface area of the LDO/fluoropolymer composite layers. The asymptotic behaviour suggests a flat surface for 40 wt.% LDO containing composite layer (see Fig. S9). With the increasing LDO content, a positive deviation can be

observed caused by the increasing surface roughness of the composite layers (Fig. S9). The Porod constant can be determined by the intercept of the fit, which constant is suitable for calculating the specific surface area (α^s) of the samples. The α^s value obtained by SAXS method presented in Table 1 is increasing with the increasing LDO content. For the 40 wt.% LDO content, the obtained surface fractal dimension (D_s) was 2 which value related for a smooth surface. When the particle content is increasing in the composite layer a higher value (2.1-2.25 for 80 wt.% and 100 wt.% LDO) was obtained for the D_s (Table 1). The scattering curves of the 40-100 wt.% LDO/fluoropolymer layers presented in Fig. 5(a) shows a characteristic peak appeared at $h = 2.66 \text{ nm}^{-1}$, which, based on calculations using the $D = 2\pi/h$ (D : diameter in nm) relationship, is indicative of the formation of scattering centers with a characteristic size of $D = 2.36 \text{ nm}$. This is assumed to be the consequence of the LDO particles in the composite layer. With the increasing LDO content less particles will be covered with fluoropolymer and surface become more roughed. This is also confirmed by the analysis of the log-log plot (Fig. 5(b)). The surface roughness and the tail end constant (K_p) were systematically increased from 0.2 to 1.54 and from 2 to 2.25 (Table. 1).

Here the obtained values for the surface were in nano dimension which refer more to the nanostructural property of the layers.

3.4. Determination of microbial adhesion capacity on the surface of composite layers

The literature data confirms our observations that with the increasing surface micro-roughness the bacterial adhesion extent to the surface increases (Taylor et al., 1998; Diaz et al., 2007; Lorenzetti et al., 2015; Zhang et al., 2013; Katsikogianni and Missirlis, 2004). Fig. 6 presents the adhesion extent of three bacterial strains on composite layers as a function of increasing LDO particle content. The optical density OD_{620} of crystal violet dye indicates that the adhesion capacity of all bacterial strains strongly depends on surface characteristics. The increasing surface roughness increases OD_{620} .

The inset of Fig. 6 shows two photos of the crystal violet coloured films. From photos we conclude that the bacterial adhesion on the relatively smooth surface of fluoropolymer (with 0 wt.% of LDO particles) was the least pronounced. This type of surface was colourless, which means that all three types of bacterial cells are not or only slightly adhered to the surface (after 18 h of incubation time at 37 °C under aerobic conditions). The measured OD₆₂₀ value of the extracted dye was between 0.01 and 0.05 (1.19×10^5 cells/cm² and 5.39×10^5 cells/cm², Fig. S10). The determined OD₆₂₀ was the highest (OD₆₂₀= 1.11-1.54) in the case of the most rough surface ($R_q = 15.3 \mu\text{m} \pm 2.04 \mu\text{m}$) with 80 wt.% of LDO content. The layer was coloured blue, and shows the presence of bacterial cells on the surface (inset of Fig. 6). The control measurements (without 18 h of bacterial incubation) indicate that the crystal violet dye do not colour the composite surface, from which follows that only the adhered bacteria were coloured.

We note that according to these microbial adhesion capacity measurements the presence of bacterial cells on the composite surface increases with the increasing LDO content and the highest bacterial adhesion was measured just for the superhydrophobic ($\theta = 156.3^\circ$), 80 wt.% LDO containing sample. The adhered cell numbers for *P. aeruginosa*, *E. coli* and *S. aureus* were 1.58×10^7 , 1.47×10^7 and 1.20×10^7 cells/cm², respectively (Fig. S10). The reason for the bacterial adhesion is the decreased coatings superhydrophobicity after immersion in water. The underwater metastability of superhydrophobic surfaces is due to three main physical mechanisms: pressurization, air diffusion, and droplet condensation. These physical mechanisms induce the wetting transition on water submerged superhydrophobic surfaces (Marmur, 2006; Cheng et al., 2019; Xue et al., 2016). Fig. S11 presents the effect of immersion time duration on the measured contact angles of superhydrophobic coating. Initially superhydrophobic surface ($\theta = 156.3^\circ$) lost their non-wetting characteristic under a relatively short period of time (120 min). However, the layers didn't lose their antibacterial

properties (see subsection 3.7). The re-dried coating has shown superhydrophobic properties again indicating the reversible nature of the process.

The results of the underwater experiments allow to conclude that the bacterial adhesion increases with the LDO loading which is due to the greater bacterial attraction on the free, uncovered LDO parts rather than the greater retention against washing/rinsing process during the experiment.

3.5. Scanning electron microscopy

The bacterial adhesion was also investigated by SEM micrographs. Fig. 7 shows a representative SEM micrographs of 80 wt.% LDO containing composite layer without (Fig. 7(a)) and with (Fig. 7(b)) adhered *S. aureus* bacteria. At this high LDO content the low energy fluoropolymer does not completely cover the surface of the LDO particles. Isolated polymer islands can be observed in Fig. 7(a) and it can be seen that the *S. aureus* bacteria obviously preferred the high energy LDO surfaces instead of the low energy polymer (Fig. 7(b)). Our results are in agreement with the literature data of Li and Logan (Li and Logan, 2004) who reported that the presence of different metal-oxides (e.g. TiO_2 , SnO_2 , Al_2O_3 , Fe_2O_3 , etc.) can increase the bacterial adhesion. Their explanation was that the negatively-charged bacteria prefer to adhere to positively charged oxide surfaces. It was confirmed that the bacteria have an attractive electrostatic contact with the positively charged LDO particles. The surface charge density of the LDO particles was estimated from the streaming potential data. 10 mL 1 wt.% LDO suspensions was titrated with 0.1 wt.% SDS negatively charged surfactant solution (Fig. 8(a)). The LDO suspension was positive and during the addition of oppositely charged SDS the streaming potential continuously decreases. Taking into account the added amount of surfactant molecules ($n_{\text{SDS}} = 0.0028 \text{ mmol}$) for the charge compensation of LDO and the mass of the titrated LDO ($= 0.1 \text{ g}$), the specific surface charge of LDO was equal to $+0.028 \text{ meq/g}$. The streaming potential of 10 mL 1 wt.% positively charged LDO suspension was also

titrated with 10^5 CFU/mL *E. coli* bacterial suspension (Fig. 8(b)) at the same experimental condition (fresh nutrient broth solution with given pH and ionic strength). Positive streaming capacity (+509 mV) is present in the initial LDO suspension, but it decreases as the number of negatively charged bacteria increases. According to the obtained electrostatic charge compensation point (0 mV streaming potential at 0.14 mL 10^5 CFU/mL *E. coli* bacteria suspension consumed), 1.4×10^5 CFU *E. coli* bacteria is electrostatically adhered to 1 g LDO particles. These results confirm that the bacterial adhesion extent depends also on the electrostatic interactions between LDO and bacterial cells (5×10^6 CFU/meq).

In the Wenzel's model, the hydrophilicity/hydrophobicity of a homogeneous substrate is amplified by decreasing/increasing surface roughness (Khan and Singh, 2013). The presented EDX measurements (Fig. S7) revealed that the coating shows superhydrophobic properties for 80 wt.% LDO content. The surface of films is heterogeneous, beside the fluoropolymer parts there are also regions of LDO particles which are not covered with a polymer. Fig. 9 presents SEM micrographs of the surface with 80 wt.% of LDO content with adhered *P. aeruginosa* (Fig. 9 a/1 and a/2), *E. coli* (Fig. 9 b/1 and b/2) and *S. aureus* (Fig. 9 c/1 and c/2) after 18 h incubation time. It can be seen that most of bacterial cells are adhered on the surface of LDO particles (Fig. 9 a/1, b/1 and c/1). More precisely, the bacteria are adhered to the lamellae, voids and gaps of LDO particles (Fig. 9 a/2, b/2 and c/2).

3.6. Determination of reactive radicals on photoreactive composite layers

At higher LDO content the polymer coverage is not complete and accessible LDO particles can be found on the surface of composite layers. Moreover, the LDO with app. 12 wt.% ZnO content shows photocatalytic activity according to the benzoic acid photodegradation tests presented in our previous paper (Deák et al., 2016).

During the photocatalytic process reactive oxygen species (ROS) were produced, which are primarily responsible for bacterial inactivation and cause an irreversible DNA degradation in

bacterial cells (Block, 2001). To detect these radicals in the presence of luminol the chemiluminescence method has been used (Min et al., 2007).

The photocatalytically generated radicals (ROS) react with luminol, produce chemiluminescence (CL) and the concentration of ROS is correlated with the amount of photoluminescence photons (Fig. S12) (Schneider, 1970). The degradation of the formed hydrogen peroxide is slow at room temperature and is measured with a luminometer (Perez-Benito, 2004). In this way the concentration of H_2O_2 is proportional to the difference of free radicals produced under appropriate illumination and consequently the ROS concentration can be expressed as equivalent H_2O_2 (mM) concentration. The equivalent concentration values of H_2O_2 (mM) as a function of illumination time is shown in Fig. 10 and exhibit an increase of producing radicals as a function of increasing illumination time. All curves saturates at larger illumination time. In the case of 80 wt.% LDO/fluoropolymer layer the amount of the ROS OH^\cdot is higher (0.34 mM H_2O_2 equivalent) than in the presence of lower LDO content composite layers (0.27; 0.19 and 0.12 mM H_2O_2 equivalent at 60, 40 and 20 wt.% LDO content) after 90 minutes of LED-light illumination. The observed saturation of the curves is the result of the undesired partial photo-degradation of the polymer binder (Veres et al., 2014). The long-term illumination impact the composition of catalyst/polymer as the photocatalyst particles became uncoated (Janovák et al., 2017) and this also caused the continuous decreasing of the measured contact angle values (Lantos et al., 2020).

In our previous works we studied the effect and durability of polymer binder on photocatalytic and structural properties (Veres et al., 2014). During these tests the nanocomposites were exposed to photoaging, which resulted in a notable increase of the photocatalytic activity, due to the partial photooxidation of polymer matrix on the surface which resulted better availability for surface photocatalyst to the model pollutant. We found that after 24 h of photoaging, the nanocomposites could perform similarly to the pure catalysts, but the mechanical stability was heavily decreased (Veres et al., 2014). Therefore,

to reduce the photodegradation of the polymer binder we applied more inert hydrophobic fluoropolymers (e.g. perfluorinated polyacrylates like poly(perfluorodecyl acrylate) (PPFDA)) as a binder material.

The above presented microbial adhesion capacity measurements show that all three types of bacterial cells are preferentially adhered to the surface of LDO photocatalyst particles which is advantageous from the viewpoint of long term- use. Namely, it is well known that the photocatalytic surfaces with generated free radicals are suitable for the continuous bacterial inactivation and inhibition of biofilm formation (Sirelkhatim et al., 2015; Achouri et al., 2018).

3.7. Bacterial cell inactivation measured by fluorescence microscopy

The LDO particles displayed photocatalytic properties (due to app. 12 wt.% of ZnO content) under LED-light illumination and produced reactive ROS. The inactivation of bacterial cells on the 80 wt.% LDO containing superhydrophobic composite layers were investigated by fluorescence microscopy. The bacterial suspension of *P. aeruginosa* was stained with Bacterial Viability staining kit and examined at the beginning of the experiment ($t=0$ min), after 1 and 2 hours of illumination with LED-light source. Fig. 11 presents the fluorescence microscopy images with the regions of the live (green) and damaged (red) *P. aeruginosa* cells on the 80 wt.% LDO containing composite layer.

At the beginning ($t=0$ min) all bacterial cells have green emission (by SYTO 9). After 120 min of illumination part of bacterial cells are damaged. Therefore, the intensity of green emission is significantly reduced due to the cell wall penetrating PI into the damaged bacterial cell wall (Fig. 11). In parallel, at the same initial time ($t=0$ min) negligible (1-2) damaged (or dead) bacterial cells were observed. The number of damaged (red emission) cells increased after 120 minutes of light exposure (Fig. 11). The percentage of live and damaged *P. aeruginosa* bacterial cells was calculated from the fluorescence microscopy images and

presented in Fig. 12. The number of live bacterial cells after 120 min of illumination was reduced by 93%. At this time, the number of damaged bacterial cells increased to 46%. The obtained bacterial inactivation is due to the generated free radicals and the photocatalysis is important in the inactivation of bacteria instead of the direct photolysis (Tallósy et al., 2016).

The fluorescent dye kit consists of two components, SYTO 9 (green) dye and propidium iodide fluorescent dye (PI, red). The SYTO 9 dye enters in both living and damaged bacterial cells, but PI dye cannot penetrate in the living bacterial cells, only if the cell wall is damaged. Although both fluorescent dyes stain the damaged cells, when used together, propidium iodide reduces the intensity of green dye emission (extinguishes) so that only the red color is visible (Tallósy et al., 2016). As a result, the use of a dye kit is excellent for the combined detection of intact (LIVE) and damaged (DEAD) cells. During photocatalytic inactivation, the wall of bacterial cells is damaged and significant degradation occurs in their peptidoglycan layer. This large extent of damage does not always allow the stained parts to be similarly visible as cells that have survived or are initially damaged.

4. Conclusion

Within this study, we develop a novel antibacterial coating composed of photoreactive LDO particles embedded in a low surface energy fluoropolymer matrix.

The surface roughness, charge, wettability and bacterial adhesion properties can be varied by adjusting the loading of LDO particles into the fluoropolymer matrix. The increasing LDO content (from 0 to 80 wt.%) increases of the surface roughness (from $0.002\ \mu\text{m} \pm 0.0002\ \mu\text{m}$ to $15.3\ \mu\text{m} \pm 2.04\ \mu\text{m}$). The composite layer (with 80 wt.% LDO content) has shown superhydrophobic and water-repellent properties with high contact angle ($156.1^\circ \pm 2.56^\circ$) and low surface free energy ($2.7\ \text{mJ/m}^2 \pm 0.65\ \text{mJ/m}^2$). On these composite layers we studied bacterial adhesion of *S. aureus*, *E. coli* and *P. aeruginosa*. We observed that the adhesion extent increases with increasing roughness of the surface layers. The reason for pronounced

bacterial adhesion is the electrostatic attraction between LDO particles and bacterial cells as well as attraction between hydrophilic LDO particles and hydrophilic bacteria. The SEM micrographs confirmed that bacteria preferably adhered to the lamellae of LDO surfaces. Due to 12 wt.% nominal content of ZnO phase in LDO particles, the composite layer has a photocatalytic property. To LDO particles adhered bacteria were photocatalytically inactivated by illuminating with LED-light for 120 min. The number of live bacteria decreases to zero with increasing illumination time.

The presence of different metal-oxides increase the bacterial adhesion since the bacteria with negative charge prefer to adhere to positively charged oxide surfaces. However, this conventional metal surfaces show very hydrophilic even superhydrophilic properties. In the case of our non-conventional composite layers with heterogeneous surface energy distribution, controllable wetting and photocatalytic properties are achieved. The bacterial adhesion preferably occurred on the lamellae of LDO photocatalyst surfaces. These composite layers can be optimized to the maximal bacterial adhesion extent. Consequently, the extent of inactivated bacteria could be maximized and ready for the inactivation with LED-light illumination. The developed composite layers can have an important application in photocatalytic air purifying and sterilizing systems and are very good for health care facilities with surfaces of antiseptic and disinfectant properties. Moreover, the performed composite layer with controllable bacterial adhesion and obvious photoreactive properties is potentially useful in the area of waste water treatment, as well.

Conflicts of interest

There are no declared conflicts.

Acknowledgements.

The authors are grateful for the financial assistance from the National Research, Development and Innovation Office (GINOP-2.3.2-15-2016-00013 and GINOP-2.1.7-15-2016-01987) and from the COST Action STSM CM1101. This paper was also supported by the UNKP-22-5 and UNKP-21-4 New National Excellence Program of the Ministry for Innovation and Technology from the source of the National Research, Development and Innovation Fund and by the János Bolyai Research Scholarship of the Hungarian Academy of Sciences. KB and KGT are very thankful for the Slovenian Research Agency for support through program P3-0388. All these supports are highly appreciated.

References

- Achouri, F., Merlin, C., Corbel, S., Alem, H., Mathieu, L., Balan, L., Medjahdi, G., Said, M. B., Ghrabi, A., Schneider, R., 2018. ZnO Nanorods with High Photocatalytic and Antibacterial Activity under Solar Light Irradiation. *Materials* 11(11), 2158.
- Bayoudh, S., Othmane, A., Ponsonnet, L., Ouada, H. B., 2008. Electrical detection and characterization of bacterial adhesion using electrochemical impedance spectroscopy-based flow chamber. *Colloids Surf. A: Physicochem. Eng. Asp.* 318, 291-300.
- Block, S. S., 2001. Disinfection, sterilization and preservation, fifth ed., Lippincott Williams & Wilkins, Philadelphia, USA.
- Bohinc, K., Dražič, G., Fink, R., Oder, M., Jevšnik, M., Nipič, D., Godič Torkar, K., Raspor, P., 2014. Metal surface characteristics dictate bacterial adhesion capacity. *Int. J. Adhes. Adhes.* 50, 265–272.
- Bohinc, K., Dražič, G., Abram, A., Jevšnik, M., Jeršek, B., Nipič, D., Kurinčič, M., Raspor, P., 2016. Available surface dictates microbial adhesion capacity. *Int. J. Adhes. Adhes.* 68, 39–46.
- Bos, R., van der Mei, H. C., Busscher, H. J., 1999. Physico-chemistry of initial microbial adhesive interactions - Its mechanisms and methods for study. *FEMS Microbiol. Rev.* 23, 179–230.
- Carja, G., Kameshima, Y., Nakajima, A., Dranca, C., Okada, K., 2009. Nanosized silver–anionic clay matrix as nanostructured ensembles with antimicrobial activity. *Int. J. Antimicrob. Agents* 34(6), 534-539.
- Chen, B., Qiu, J., Sakai, E., Kanazawa, N., Liang, R., Feng, H., 2016. Robust and superhydrophobic surface modification by a “paint+adhesive” method: applications in self-cleaning after oil contamination and oil-water separation. *ACS Appl. Mater. Interfaces*, 8(27), 17659–17667.

- Cheng, Y., Feng, G., Moraru, C. I., 2019. Micro- and Nanotopography Sensitive Bacterial Attachment Mechanisms: A Review. *Front. Microbiol.* 10, 191-208.
- Chibowski, E., 2003. Surface free energy of a solid from contact angle hysteresis. *Adv. Colloid Interface Sci.* 103, 149–172.
- Chung, C.-J., Lin, H.-I., Tsou, H.-K., Shi, Z.-Y., He, J.-L., 2008. An antimicrobial TiO₂ coating for reducing hospital-acquired infection. *J. Biomed. Mater. Res. Part B Appl. Biomater.* 85B(1), 220–224.
- Deák, Á., Janovák, L., Tallósy, Sz. P., Bitó, T., Sebők, D., Buzás, N., Pálinkó, I., Dékány, I. (2015). Spherical LDH–Ag⁺–Montmorillonite Heterocoagulated System with a pH-Dependent Sol–Gel Structure for Controlled Accessibility of AgNPs Immobilized on the Clay Lamellae. *Langmuir*, 31(6), 2019–2027.
- Deák, Á., Janovák, L., Csapó, E., Ungor, D., Pálinkó, I., Puskás, S., Ördög, T., Ricza, T., Dékány, I., 2016. Layered double oxide (LDO) particle containing photoreactive hybridlayers with tunable superhydrophobic and photocatalytic properties. *Appl. Surf. Sci.* 389, 294–302.
- Diaz, C., Schilardi, P. L., Salvarezza, R. C., Fernández Lorenzo de Mele, M., 2007. Nano/Microscale Order Affects the Early Stages of Biofilm Formation on Metal Surfaces, *Langmuir* 23, 11206-11210.
- Drelich, J., 2013. Guidelines to measurements of reproducible contact angles using a sessile-drop technique. *Surf Innov.* 1(4), 248-254.
- Dunne, C. P., Keinänen-Toivola, M. M., Kahru, A., Teunissen, B., Olmez, H., Gouveia, I., Melo, L., Murzyn, K., Modic, M., Ahonen, M., Askew, P., Papadopoulos, T., Adlhart, C., Crijns, F. R. L., 2017. Anti-microbial coating innovations to prevent infectious diseases (AMiCI): Cost action ca15114. *Bioengineered* 8:6, 679-685.
- Dunne, S. S., Ahonen, M., Modic, M., Crijns, F. R. L. , Keinänen-Toivola, M. M., Meinke, R., Keevil, C. W., Gray, J., O’Connell, N. H., Dunne, C. P., 2018. Specialized cleaning

associated with antimicrobial coatings for reduction of hospital-acquired infection: opinion of the COST Action Network AMiCI (CA15114). *J. Hosp. Infect.* 99, 250-255.

Fateh, R., Dillert, R., Bahnemann, D., 2014. Self-Cleaning Properties, Mechanical Stability, and Adhesion Strength of Transparent Photocatalytic TiO₂–ZnO Coatings on Polycarbonate. *ACS Appl. Mater. Interfaces* 6(4), 2270–2278.

Fresno, F., Portela, R., Suárez, S., Coronado, J. M., 2014. Photocatalytic materials: recent achievements and near future trends. *J. Mater. Chem. A* 2, 2863-2884.

Fujishima, A., Honda, K., 1972. Electrochemical photolysis of water at a semiconductor electrode. *Nature* 238, 37–38.

Ghosh, R., Swart, O., Westgate, S., Miller, B. L., Yates, M. Z., 2019. Antibacterial copper-hydroxyapatite composite coatings via electrochemical synthesis. *Langmuir* 35(17), 5957-5966.

Hasan, J., Raj, S., Yadav, L., Chatterjee, K., 2015. Engineering a Nanostructured “Super Surface” with Superhydrophobic and Superkilling Properties. *RSC Adv.* 5 (56), 44953–44959.

Herrald, P. J., Zootolla, E. A., 1988. Scanning electron microscopic examination of *Yersinia enterocolitica* attached to stainless steel at elevated temperature and pH values. *J. Food Sci.* 51, 445–448.

Janovák, L., Deák, Á., Tallósy, Sz. P., Sebők, D., Csapó, E., Bohinc, K., Abram, A., Pálinkó, I., Dékány, I., 2017. Hydroxyapatite-enhanced structural, photocatalytic and antibacterial properties of photoreactive TiO₂/HAp/polyacrylate hybrid thin films. *Surf. Coat. Technol.* 326, 316-326.

Katsikogianni, M., Missirlis, Y. F., 2004. Concise review of mechanisms of bacterial adhesion to biomaterials and of techniques used in estimating bacteriamaterial interactions. *Eur Cell Mater* 8, 37-57.

Khan, S., Singh, J. K., 2013. Wetting transition of nanodroplets of water on textured surfaces: a molecular dynamics study. *Mol Simul*, 40(6), 458-468.

Kovačević, D., Pratnekar, R., Godič Torkar, K., Salopek, J., Dražić, G., Abram, A., Bohinc, K., 2016. Influence of Polyelectrolyte Multilayer Properties on Bacterial Adhesion Capacity. *Polymers* 8(10), 345.

Lantos, E., Mérai, L., Deák, Á., Gómez-Pérez, J., Sebők, D., Dékány, I., Kónya, Z., Janovák, L., 2020. Preparation of sulfur hydrophobized plasmonic photocatalyst towards durable superhydrophobic coating material. *J Mater Sci Technol*, 41, 159–167.

Li, B., Logan, B. E., 2004. Bacterial adhesion to glass and metal-oxide surfaces. *Colloids Surf. B* 36, 81–90.

Li, R., Boudot, M., Boissière, C., Grosso, D., Faustini, M., 2017. Suppressing Structural Colors of Photocatalytic Optical Coatings on Glass: The Critical Role of SiO₂. *ACS Appl. Mater. Interfaces*, 9(16), 14093-14102.

Li, Y., Wu, S., Wu, J., Hu, Q., Zhou, C., 2020. Photothermocatalysis for efficient abatement of CO and VOCs. *J. Mater. Chem. A* 8, 8171-8194.

Liu, K., Jiang, L., 2011. Metallic surfaces with special wettability. *Nanoscale* 3, 825-838.

Lorenzetti, M., Dogša, I., Stošicki, T., Stopar, D., Kalin, M., Kobe, S., Novak, S., 2015. The Influence of Surface Modification on Bacterial Adhesion to Titanium-Based Substrates. *ACS Appl. Mater. Interfaces* 7, 1644-1651.

Marmur, A., 2006. Underwater Superhydrophobicity: Theoretical Feasibility. *Langmuir* 24, 1400–1402.

McHale, G., Shirtcliffe, N. J., Newton, M. I., 2004. Contact-Angle Hysteresis on Super-Hydrophobic Surfaces. *Langmuir*, 10146-10149.

Min, L., Wu, X.-Z., Tetsuya, S., Inoue, H., 2007. Time-resolved chemiluminescence study of the TiO₂ photocatalytic reaction and its induced active oxygen species. *Luminescence* 22, 105–112.

- Nosonovsky, M., Bhushan, B., 2009. Superhydrophobic Surfaces and Emerging Applications: Non-Adhesion, Energy, Green Engineering. *Curr. Opin. Colloid Interface Sci.* 14 (4), 270–280.
- Owens, D. K., Wendt, R. C., 1969. Estimation of the surface free energy of polymers. *J. Appl. Polym. Sci.* 13(8), 1741–1747.
- Perez-Benito, J. F., 2004. Iron(III)-hydrogen peroxide reaction: kinetic evidence of a hydroxylmediated chain mechanism. *J. Phys. Chem. A* 108, 4853–4858.
- Raghunath A., Perumal, E., 2017. Metal oxide nanoparticles as antimicrobial agents: a promise for the future. *Int. J. Antimicrob. Agents* 49(2), 137-152.
- Rossi, S., Deflorian, F., Scrinzi, E., 2009. Reduction of aesthetical properties of organic coatings caused by mechanical damage. *Mater. Des.* 30, 1511–1517.
- Saxena, N., Naik, T., Paria, S., 2017. Organization of SiO₂ and TiO₂ Nanoparticles into Fractal Patterns on Glass Surface for the Generation of Superhydrophilicity. *J. Phys. Chem. C* 121(4), 2428–2436.
- Schneider, H. W., 1970. A new, long-lasting luminol chemiluminescent cold light. *Journal of Chemical Education*, 47(7), 519–522.
- Sedelnikova, M. B., Komarova, E. G., Sharkeev, Y. P., Ugodchikova, A. V., Tolkacheva, T. V., Rau, J. V., Buyko, E. E., Ivanov, V. V., Sheikin, V. V., 2019. Modification of titanium surface via Ag-, Sr- and Si-containing micro-arc calcium phosphate coating. *Bioactive Materials* 4, 224–235.
- Selim, M. S., El-Safty, S. A., Shenashen, M. A., Higazy, S. A., Elmarakbic, A., 2020. Progress in biomimetic leverages for marine antifouling using nanocomposite coatings. *J. Mater. Chem. B* 8, 3701-3732.
- Sirelkhatim, A., Mahmud, S., Seeni, A., Kaus, N. H. M., Ann, L. C., Bakhori, S. K. M., Hasan, H., Mohamad, D., 2015. Review on Zinc Oxide Nanoparticles: Antibacterial Activity and Toxicity Mechanism. *Nano-Micro Lett* 7(3), 219–242.

- Tallósy, S. P., Janovák, L., Nagy, E., Deák, Á., Juhász, Á., Csapó, E., Buzás, N., Dékány, I., 2016. Adhesion and inactivation of Gram-negative and Gram-positive bacteria on photoreactive TiO₂/polymer and Ag–TiO₂/polymer nanohybrid films. *Appl. Surf. Sci.* 371, 139–150.
- Tallósy, Sz. P., Janovák, L., Ménesi, J., Nagy, E., Juhász, Á., Balázs, L., Deme, I., Buzás N., Dékány, I., 2014a. Investigation of the antibacterial effects of silver modified TiO₂ and ZnO plasmonic photocatalysts embedded in polymer thin films. *Environ. Sci. Pollut. Res.* 21(19), 11155-11167.
- Tallósy, Sz. P., Janovák, L., Ménesi, J., Nagy, E., Juhász, Á., Dékány, I., 2014b. LED-light Activated Antibacterial Surfaces Using Silver-modified TiO₂ Embedded in Polymer Matrix. *J. Adv. Oxid. Technol.* 17, 9-16.
- Taylor, R. L., Verran, J., Lees, G. C., Ward, A. J. P., 1998. The influence of substratum topography on bacterial adhesion to polymethyl methacrylate. *J. Mater. Sci. Mater. Med.* 9, 17-22.
- Torchinsky, I., Rosenman, G., 2009. Wettability Modification of Nanomaterials by Low-Energy Electron Flux. *Nanoscale Res. Lett.* 4(10), 1209–1217.
- Tung, W. S., Daoud, W. A., 2009. Photocatalytic self-cleaning keratins: A feasibility study. *Acta Biomaterialia*, 5(4), 50-56.
- Tung, W. S., Daoud, W. A., 2011. Self-cleaning fibers *via* nanotechnology: a virtual reality. *J. Mater. Chem.* 21, 7858.
- Veres, Á., Ménesi, J., Juhász, Á., Berkesi, O., Ábrahám, N., Bohus, G., Oszkó, A., Pótári, G., Buzás, N., Janovák, L., Dékány, I., 2014. Photocatalytic performance of silver-modified TiO₂ embedded in poly(ethyl-acrylate-co-methyl metacrylate) matrix. *Colloid. Polym. Sci.* 292, 207–217.

Veres, Á., Rica, T., Janovák, L., Dömök, M., Buzás, N., Zöllmer, V., Seemann, T., Richardt, A., Dékány, I., 2012. Silver and gold modified plasmonic TiO₂ hybrid films for photocatalytic decomposition of ethanol under visible light. *Catal. Today* 181, 156–162.

Xie, X., Mao, C., Liu, X., Tan, L., Cui, Z., Yang, X., Zhu, S., Li, Z., Yuan, X., Zheng, Y., Yeung, K. W. K., Chu, P. K., Wu, S., 2018. Tuning the Bandgap of Photo-Sensitive Polydopamine/Ag₃PO₄/Graphene Oxide Coating for Rapid, Noninvasive Disinfection of Implants. *ACS Cent. Sci.* 4(6), 724–738.

Xue, C.-H., Li, M., Guo, X.-J., Li, X., An, Q.-F., Jia, S.-T., 2017. Fabrication of superhydrophobic textiles with high water pressure resistance. *Surf. Coat. Technol.* 310, 134–142.

Xue, Y., Lv, P., Lin, H., Duan, H., 2016. Underwater Superhydrophobicity: Stability, Design and Regulation, and Applications. *App Mech Rev* 68(3), 030803.

Zhang, X., Wang, L., Levänen, E., 2013. Superhydrophobic surfaces for the reduction of bacterial adhesion. *RSC Adv.* 3, 12003-12020.

Zhang, Z., Chen, B., Lu, B., Wu, H., Wu, H., Jiang, S., Chai, G., 2017. A novel thermo-mechanical anti-icing/de-icing system using bi-stable laminate composite structures with superhydrophobic surface. *Compos. Struct.* 180, 933-943.

Zhu, J., Uliana, A., Wang, J., Yuan, S., Li, J., Tian, M., Simoens, K., Volodin, A., Lin, J., Bernaerts, K., Zhang, Y., Van der Bruggen, B., 2016. Elevated salt transport of antimicrobial loose nanofiltration membranes enabled by copper nanoparticles *via* fast bioinspired deposition. *J. Mater. Chem. A* 4(34), 13211–13222.

Zisman, W. A., 1964. Relation of the equilibrium contact angle to liquid and solid construction, *Adv. Chem. Ser.* 43 (1964) 1-51.

Figures

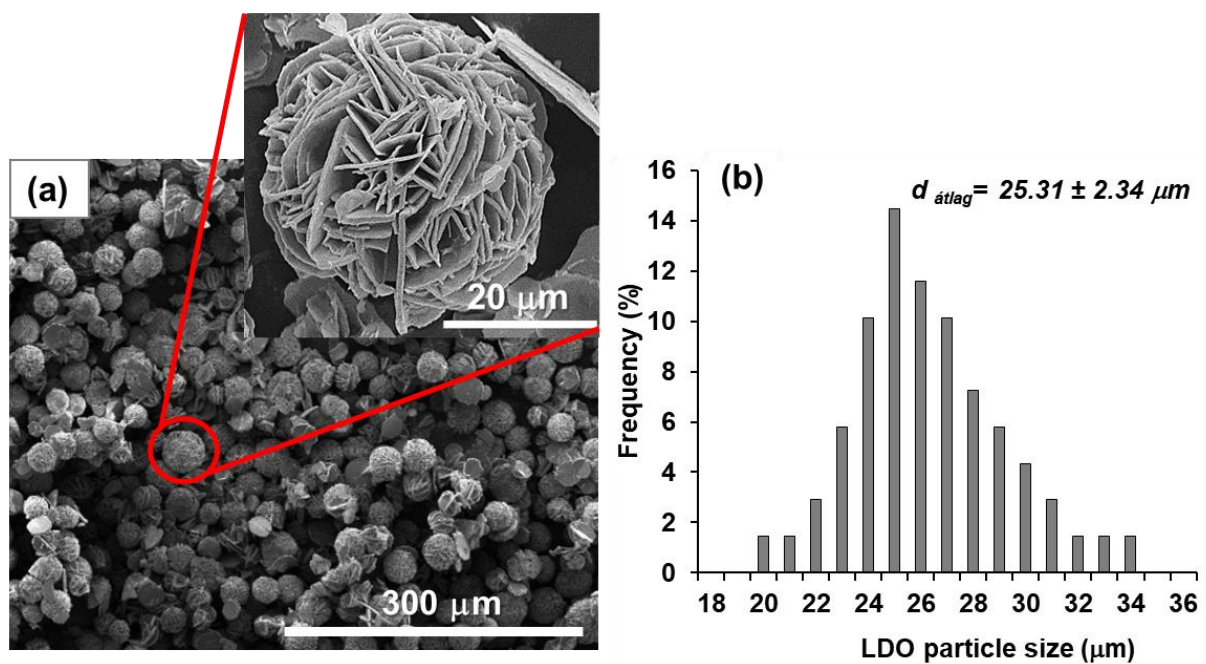


Fig. 1. SEM micrograph (a) and the corresponding size distribution (b) of the LDO photocatalyst particles used for the roughening of the composites.

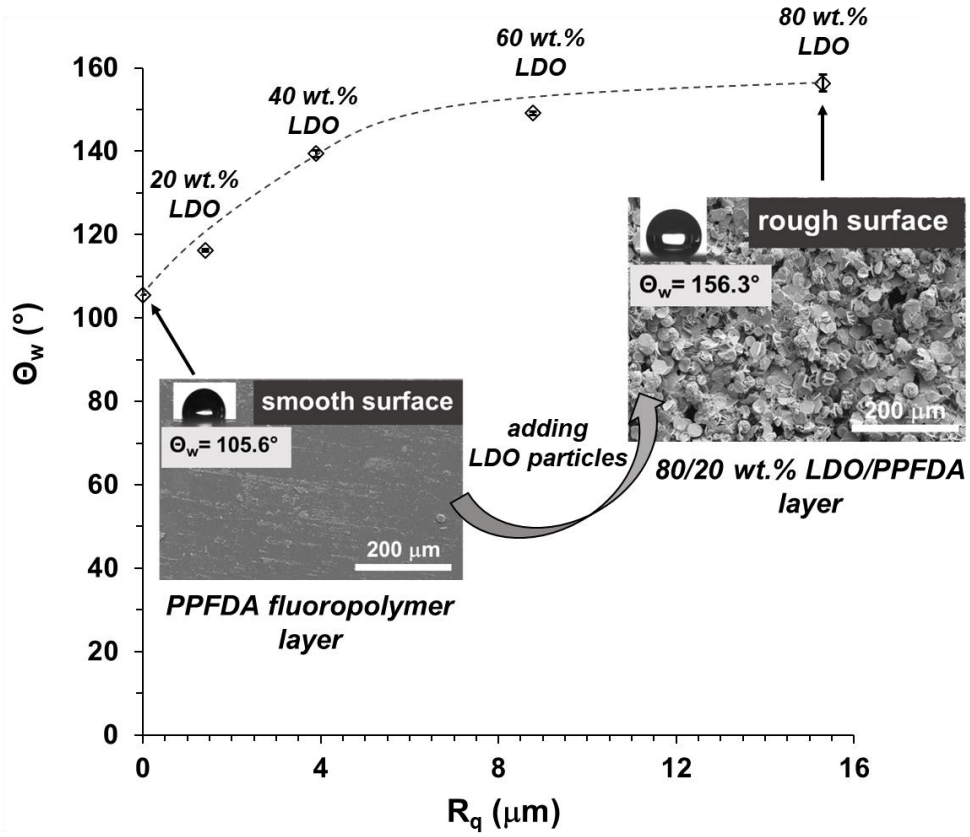


Fig 2. The contact angle values (Θ_w) of composite layers as a function of surface roughness (R_q), ($T = 25\text{ }^\circ\text{C} \pm 0.5\text{ }^\circ\text{C}$). Inset: topographies of surfaces with extreme roughness (rough and smooth) with their water contact angle (Θ_w) values and photographs of the liquid droplets on the composite layers. Smooth surface is composed of only fluoropolymer (PPFDA). Rough surface is composed of 80 wt.% LDO and 20 wt.% PPFDA.

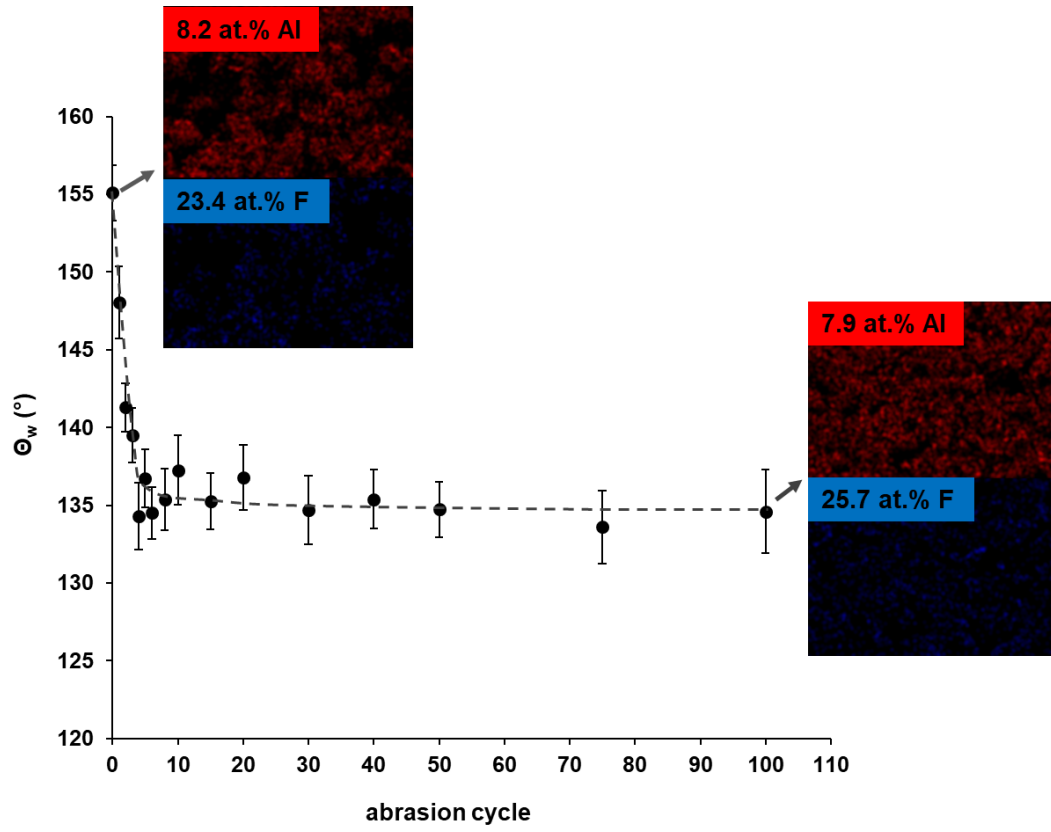


Fig. 3. θ_w as a function of abrasion cycle applied on composite layer composed of 80 wt.% LDO. Inset: the element distribution for Al (red) and F (blue) for the initial composite layer and after 100 abrasion cycles. The dashed line is a guide to eyes.

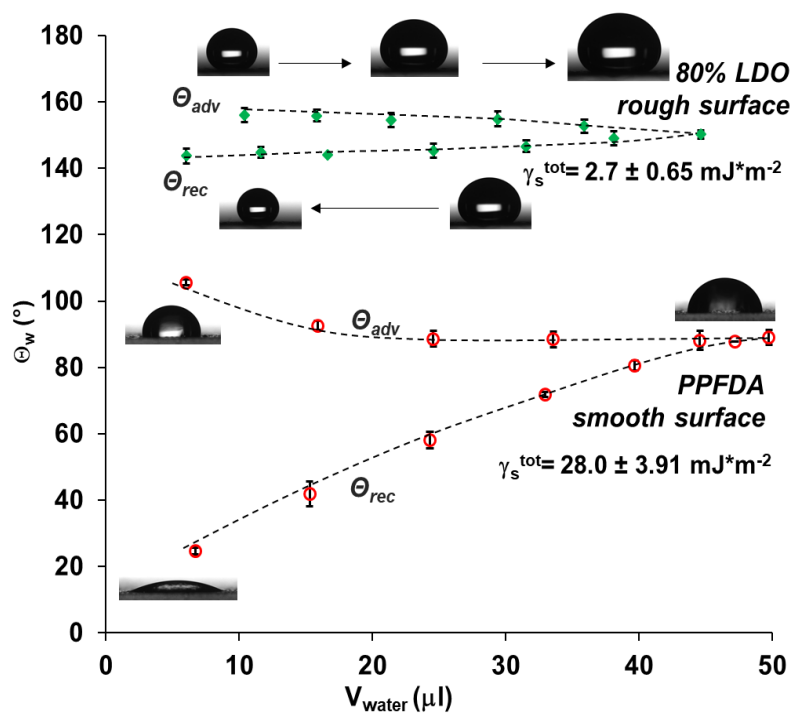


Fig. 4. Advancing (θ_{adv}) and receding (θ_{rec}) water contact angles (θ_w) as a function of water droplet volume (V_{water}) for smooth PPFDA fluoropolymer surface (red) and LDO roughened (80 wt.% LDO) layers (green). The photos of the liquid droplet and on the composite layers and the surface free energy (γ_s^{tot}) values are also presented.

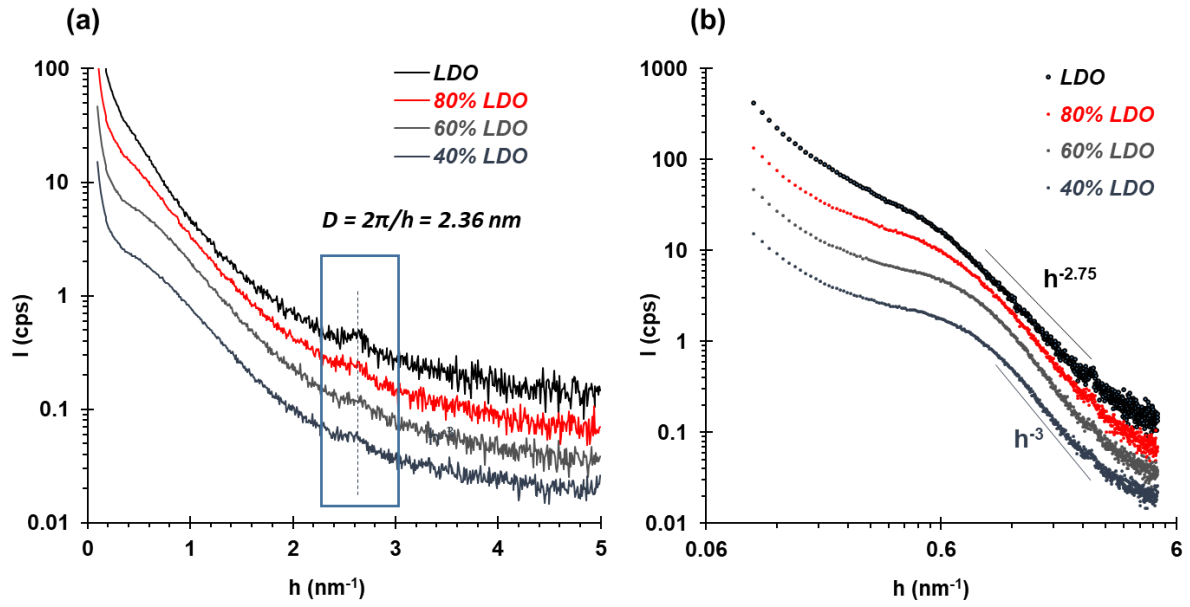


Fig 5. SAXS curves (a) and log-log plot representation (b) of the composite layers with 40, 60, 80 and 100 wt.% LDO content. (Dashed lines indicate the power-law exponents for calculating the surface fractal dimensions.)

Table 1. SAXS parameters* of the composite layers with 40, 60, 80 and 100 wt.% LDO content.

Samples	D_s	Porod constant K_p	a^s (m ² /g)	Surface roughness (nm)	L_c (nm)
100% LDO	2.15	4.86	8.2	1.54	8.83
80% LDO	2.1	3.64	7.4	0.3	6.72
60% LDO	2.05	3.36	7.1	0.2	5.44
40% LDO	2	2.65	5.6	0.2	4.71

* surface fractal dimension (D_s), tail end constant (K_p), specific surface area (a^s), correlation length (L_c).

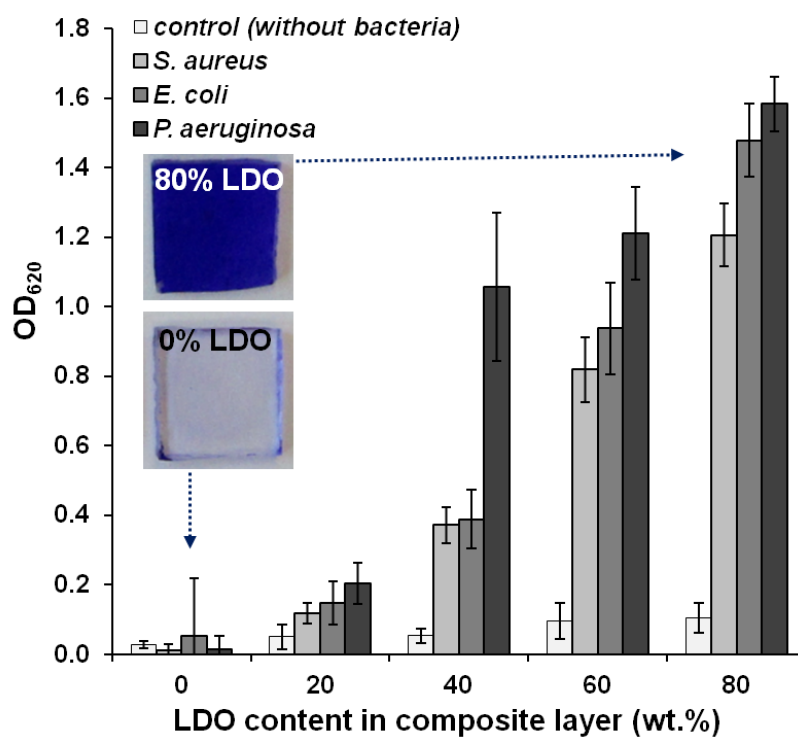


Fig. 6. The microbial adhesion capacity determined with OD₆₂₀ of crystal violet dye released from stained bacterial cells adhering to the surface of the composite layers with different LDO content. The inset shows the crystal violet coloured composite layers (with 0 and 80 wt.% LDO content).

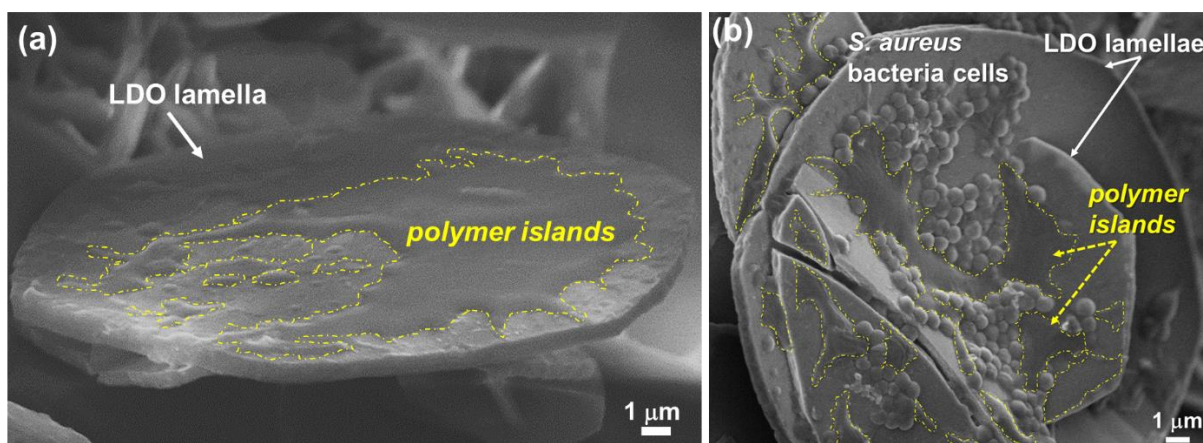


Fig. 7. SEM micrographs of composite layer with a single LDO lamella partially covered by polymer islands (a) and the colony of the adhered *S. aureus* bacteria on the hydrophilic LDO lamellae covered with the unfavorable hydrophobic polymer islands (b).

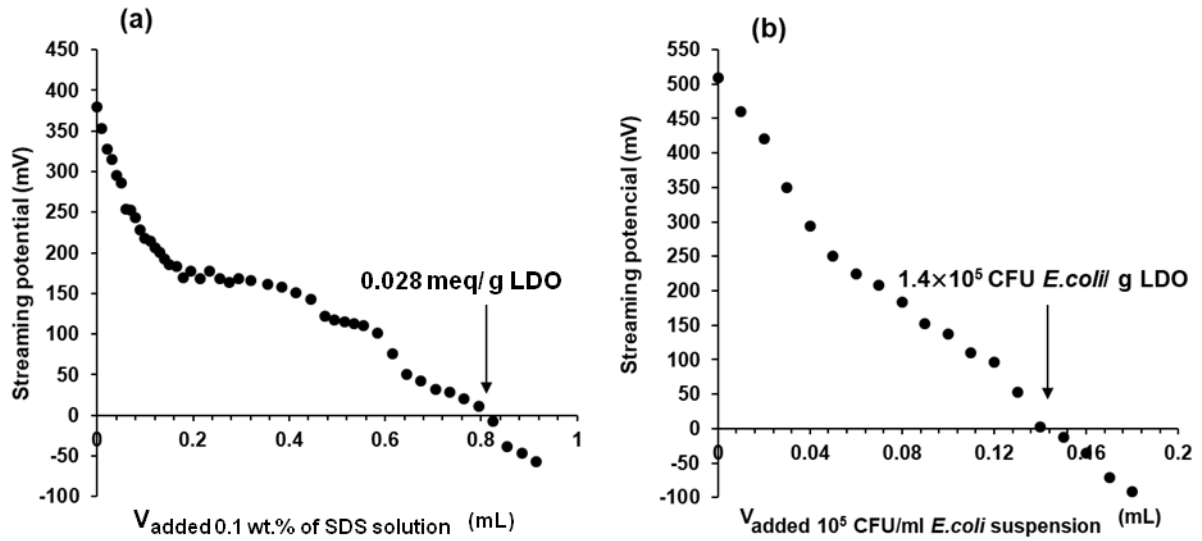


Fig. 8. The charge titration curves of 1 wt.% positively charged LDO suspension (pH = 4.5) with 0.1 wt.% of negatively charged SDS surfactant solution (a) and 10^5 CFU/mL *E. coli* suspension (b).

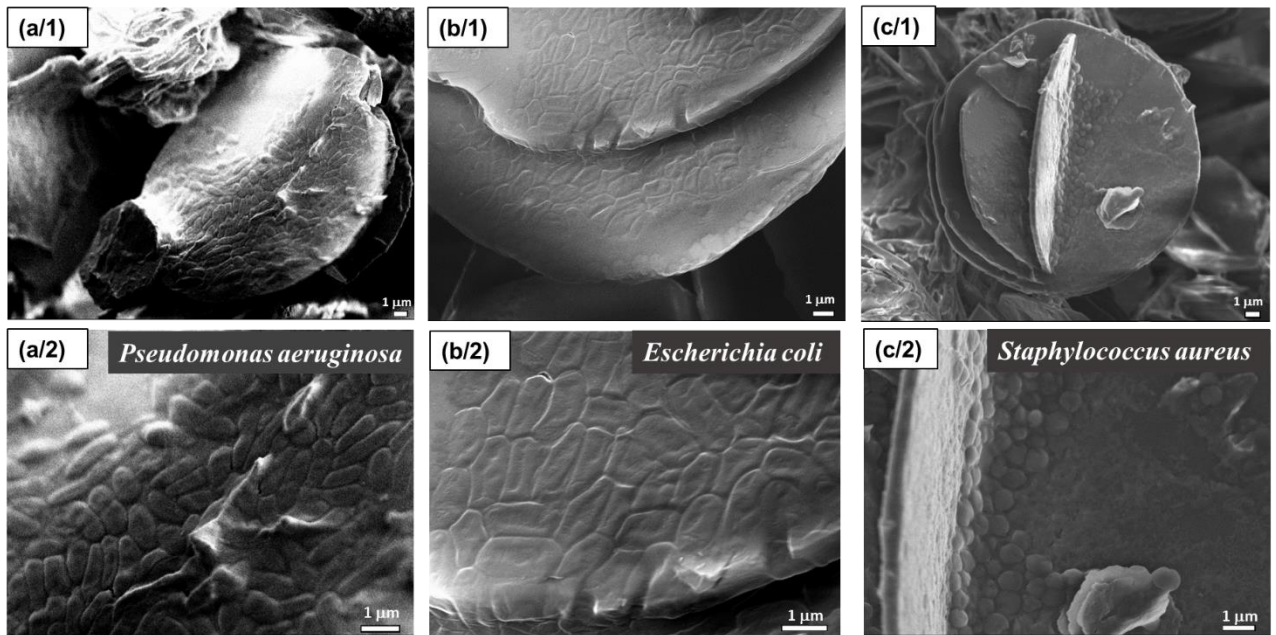


Fig. 9. SEM micrographs of the adhered *P. aeruginosa* (a/1 and a/2), *E. coli* (b/1 and b/2) and *S. aureus* (c/1 and c/2) bacteria on the 80 wt.% LDO containing composite layers after 18 h of bacterial incubation. The majority of bacteria are present on the surface of hydrophilic, high energy LDO particles (see a/2, b/2 and c/2).

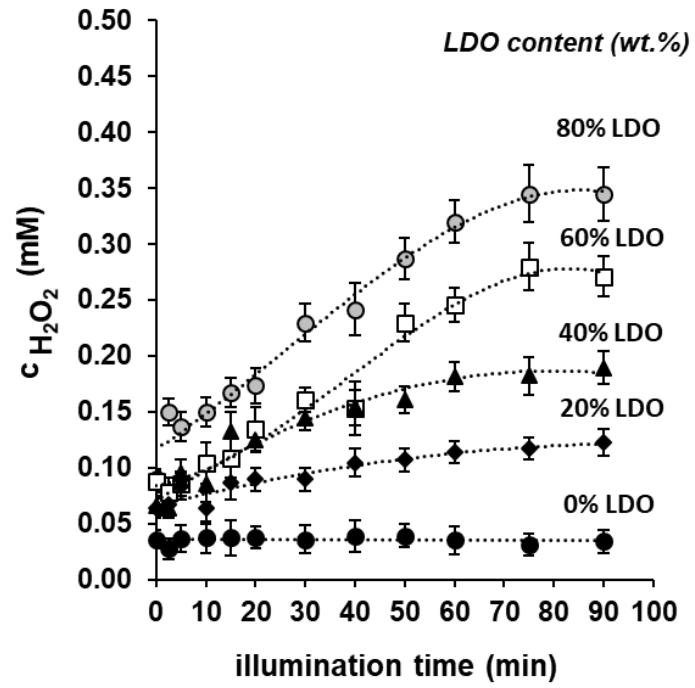


Fig. 10. The equivalent H_2O_2 concentration ($c_{H_2O_2}$) dependence on illumination time for different LDO content is shown.

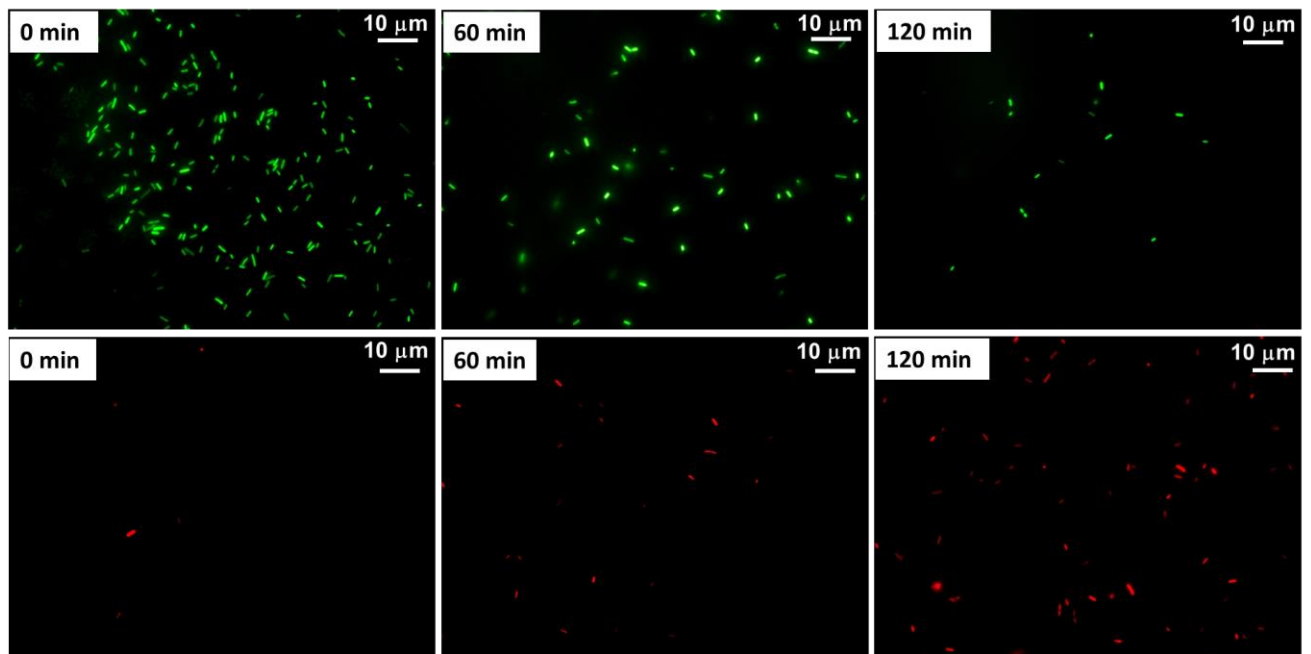


Fig. 11. The viability of *P. aeruginosa* bacterial cells evaluated with fluorescence microscope.

The green parts correspond to live bacteria whereas the red parts corresponds to damaged bacterial cells on the 80 wt.% LDO containing composite layers at the beginning ($t=0$ min) and after 1 and 2 hours of illumination time. The LED-light illumination has wavelength of

$\lambda_{\text{max}}=405$ nm. The inserted scale bars are 10 μm.

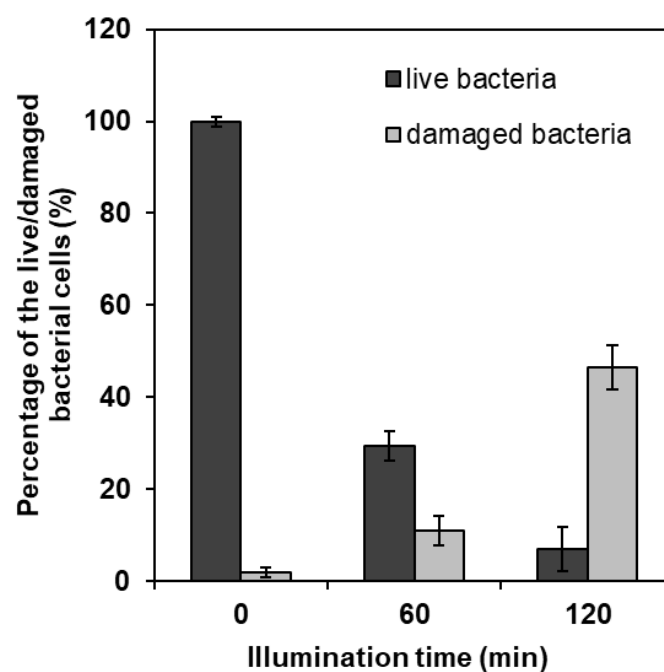


Fig. 12. The percentage of the live and damaged *P. aeruginosa* bacteria adhered on the composite layer as a function of illumination time calculated from the fluorescence microscopy images.

Synthesis of self-cleaning and photoreactive spherical layered double oxide/polymer composite thin layers: biofouling and inactivation of bacteria

Ágota Deák^a, László Janovák^{a,*}, Szabolcs Péter Tallósy^b, Karmen Godič-Torkar^c, Anže Abram^{d,e}, Imre Dékány^a, Dániel Sebők^f, Klemen Bohinc^{c,*}

^aUniversity of Szeged, Department of Physical Chemistry and Materials Science, H-6720, Rerrich Béla tér 1, Szeged, Hungary

^bUniversity of Szeged, Institute of Surgical Research, H-6724, Pulz u. 1, Szeged, Hungary

^cUniversity of Ljubljana, Faculty of Health Sciences, Zdravstvena pot 5, 1000 Ljubljana, Slovenia

^dDepartment for Nanostructured Materials, 'Jožef Stefan' Institute, Jamova cesta 39, 1000 Ljubljana, Slovenia

^eJožef Stefan International Postgraduate School, Jamova cesta 39, 1000 Ljubljana, Slovenia

^fDepartment of Applied and Environmental Chemistry, University of Szeged, H-6720, Rerrich Béla tér 1., Szeged, Hungary

*Corresponding author. Tel.: +36 62 544 209; fax: +36 62 544 042.

E-mail address: janovakl@chem.u-szeged.hu (L. Janovák), klemen.bohinc@zf.uni-lj.si (K. Bohinc)

Abstract

Layered double oxide (LDO) photocatalyst microparticles were synthesized with special radial lamellar orientation. We presented that the $25.31 \pm 2.34 \mu\text{m}$ LDO particles with rough surface can be incorporated in fluoropolymer solution and resulted a composite layer with dual superhydrophobic and photocatalytic properties with high bacterial adhesion and inactivation

ability. Next the LDO content in the composite layers were systematically increased (0, 20, 40, 60, 80 and 100 wt.% LDO) which facilitated the surface adhesion of bacteria by electrostatic interactions. The structure of the initial LDO and LDO/fluoropolymer composites was verified by small angle X-ray scattering (SAXS), XRD and SEM measurements. We showed that the surface roughness and hydrophobicity increase with increasing LDO loading. At 80/20 wt.% LDO/fluoropolymer ratio the apparent surface energy was low enough to obtain a superhydrophobic surface ($\theta_w = 156.3^\circ$ and $\gamma_s^{tot} = 2.7 \text{ mJ/m}^2$). The bacterial adhesion extent on LDO/fluoropolymer composite layers increases with increasing LDO content because the adhesion takes place preferentially to LDO lamellae. The reason for this pronounced adhesion of negatively charged and hydrophilic bacteria onto positively charged and hydrophilic LDO surfaces is the electrostatic attraction between oppositely charged surfaces. The bacterial adhesion was detected by scanning electron and fluorescence microscopy and crystal violet staining assay. Finally, the adhered bacteria were inactivated by the LED-light illumination due to photoreactivity of LDO particles containing 12 wt.% of ZnO phase.

Keywords: layered double oxide (LDO), composite layers, superhydrophobicity, photoreactive surfaces, bacterial adhesion.

1. Introduction

An increasing application of different nano- and microparticles for antimicrobial coatings has been reviewed in the fields of medicine, biology and technology (Zhu et al., 2016; Ghosh et al., 2019). A large part of research related to antimicrobial surfaces was dedicated to hospitals and other health care facilities (Dunne et al., 2018; Chung et al., 2008), where it is demanded that the coated surfaces have well-defined antiseptic and disinfectant properties. Additional self-cleaning properties of newly developed coatings can increase their value and usefulness (Selim et al., 2020; Dunne et al., 2017). Therefore, the study of self-cleaning antimicrobial surfaces has received considerable attention and became an important research topic (Tung et al., 2009;

Carja et al., 2009; Sedelnikova et al., 2019; Tung et al., 2011). According to literature, superhydrophobic surfaces with a water contact angle (θ) greater than 150° are one form of self-cleaning surfaces. Walls, paints, textiles, and window glass with self-cleaning property are only a few of the applications for superhydrophobic surfaces (Chen et al., 2016; Saxena et al., 2017; Li et al., 2017; Xue et al., 2017). In general, to achieve superhydrophobic surfaces, the surface roughness should be increased, and the surface energy should be reduced (Liu et al., 2011; Zhang et al., 2017). Increasing the roughness of a hydrophobic solid surface ($\theta > 90^\circ$) could result higher contact angle and superhydrophobic surface ($\theta > 150^\circ$). The conventional superhydrophobic surfaces with antibacterial activity show roughness at both nano- and micro-scale. It is more effective to create water repellent surfaces with roughness scales smaller than 500 nm to prevent potential bacterial trapping and inclusion effects (Hasan et al., 2015; Nosonovsky et al., 2009).

The photocatalytic coatings are another group of self-cleaning surfaces, which is able to decompose various organic materials under light exposure (Li et al., 2020; Fresno et al., 2014). Semiconductor particles (*e.g.* TiO_2 or ZnO) show photocatalytic activity (Fateh et al., 2014) and produce highly reactive oxygen species like superoxide radical ion ($\text{O}_2^{\cdot-}$), hydrogen peroxide (H_2O_2), or hydroxyl radical (HO^\cdot) (Fujishima and Honda, 1972) under light exposure. These reactive species are able to inactivate both organic compounds and the microorganisms (Veres et al., 2012; Tallósy et al., 2014).

Bacterial adhesion to different surfaces is a complex phenomenon that is influenced by the physical and chemical characteristics of the surfaces as well as the bacterial cells themselves (Bayoudh et al., 2008; Xie et al., 2018). Surface properties such as surface roughness, charge, and degree of hydrophobicity influence the intensity of bacterial adhesion (Bos et al., 1999; Bohinc et al., 2014, 2016). Beside the surface properties, the intensity of bacterial adhesion is also influenced by the charge of the bacterial cell wall, hydrophobicity, flagellation and motility (Bos et al., 1999). Environmental factors (*e.g.* temperature, pH, nutrient composition, etc.)

enhance the bacterial adhesion and the growth of biofilms (Herrald and Zootolla, 1988; Raghunath and Perumal, 2017).

In our previous work (Deák et al., 2016) we have presented the synthesis and advantage of inorganic/organic hybrid layers with dual superhydrophobic and photoreactive properties. These superhydrophobic layers were synthesized using ~25 μm layered double oxide (LDO) photocatalyst particles and low surface energy poly(perfluorodecyl acrylate) (PPFDA) fluoropolymer binder material. The application of PPFDA resulted a decrease in the surface free energy of the hydrophilic LDO. The structured surface LDO photocatalyst particles with ~12% nominal ZnO content (Deák et al., 2016) were synthesized from layer double hydroxide (LDH) spheres. The morphological characteristics of LDH are significantly affected by the synthesis conditions: at alkaline pH values ($\text{pH} > 8$) lamellar LDH is formed, whereas at acidic pH values ($\text{pH} = 3$), in the presence of urea, spherical LDH can be obtained (Deák et al. 2015). The determined excitation wavelength and the calculated band gap energy values were 386 nm and 3.23 eV, respectively. It was found that the simultaneous superhydrophobic behaviour ($\theta > 150^\circ$) and the satisfactory photocatalytic properties of the thin film occurred at 80-90 wt% LDO content. The determined surface free energy value of the superhydrophobic hybrid layer with 80 wt% LDO content was 11.8 mJ/m^2 . In the benzoic acid photodegradation test experiments, the hybrid layers with 80-90 wt% LDO content photodegraded 22-24% of the initial test molecule concentration (0.17 g/L) under UV-A ($\lambda_{\text{max}} = 365 \text{ nm}$) illumination.

Thus, based on these results, the main goal of the present work is to study the bacterial adhesion and photocatalytic inactivation ability on these composite. The bacterial adhesion extent was investigated using the crystal violet staining assay. The LDO lamellae surface with adhered bacteria was examined using scanning electron microscopy micrographs. With adjusting the loading of spherical LDO particles into composite layers the surface roughness, the surface charge density, the wetting properties and thus the bacterial adhesion capacity are controlled. The surface roughness was investigated by profilometric measurements and the surface charge

was determined with the manual titration using a Particle Charge Detector. Water contact angle measurements were used to estimate the hydrophobicity of the composite layers. To inactivate the adhered bacteria the photoreactive LDO/fluoropolymer composite surface was illuminated by LED-light and the photoreactivity was also evidenced by luminometric measurements. Fluorescence microscopy measurements were used to detect live and dead bacteria on the composite layer.

2. Materials and methods

2.1. Preparation of LDO particles

The layered double oxide (LDO) was prepared by calcination process of the spherical layered double hydroxide (LDH) (Deák et al., 2016). LDH was synthesised by a simply co-precipitation method using magnesium nitrate hexahydrate ($\text{Mg}(\text{NO}_3)_2 \cdot 6\text{H}_2\text{O}$, 98%; Sigma-Aldrich, United Kingdom), zinc nitrate hexahydrate ($\text{Zn}(\text{NO}_3)_2 \cdot 6\text{H}_2\text{O}$, 99%; Fluka Chemika, Croatia), and aluminium nitrate nonahydrate ($\text{Al}(\text{NO}_3)_3 \cdot 9\text{H}_2\text{O}$, 99,7%; Molar Chemicals KFT, Hungary) as precursors. The molar ratio of $(\text{Zn} + \text{Mg}):\text{Al}$ was 2:1 and the $\text{Zn}:\text{Mg}$ was 1:8. During the process, urea ($(\text{NH}_2)_2\text{CO}$, 98%, Sigma-Aldrich, Germany) was used as a gas bubble forming agent. The resulting precipitate was aged at 98 °C, then centrifuged, washed with distilled water, and dried in a 60 °C oven (overnight). The resulted LDH powder was calcinated 2 hours at 600 °C to obtain LDO particles. The XRD patterns presents the formation of oxide phase for LDO see in *Supporting Information*, Fig. S1.

2.2. Synthesis of fluoropolymer binder

1H, 1H, 2H, 2H-perfluorodecyl acrylate (PFDA) monomer and 2-dimethoxy-2-phenylacetophenone (Irgacure 651) initiator were used for the synthesis of fluoropolymer. The initiator and monomer were obtained from Aldrich Chemical and were used without further purification. The fluoropolymer sample of poly(1H, 1H, 2H, 2H-perfluorodecyl acrylate)

(PPFDA) was dissolved in butyl-acetate (10 wt.% polymer solution) and used to produce composite layers. Molecular weight determination of synthesized fluoropolymer was performed by using dynamic light scattering (DLS) measurements. The weight average (M_w) molecular weight of the obtained PPFDA was 56 kDa (see in *Supporting Information*, Fig. S2).

2.3. Preparation of LDO/fluoropolymer composites

The LDO containing composite layers were prepared on $5 \times 5 \text{ cm}^2$ glass plates using a gravity feed airbrush (ChroMax BD-203) sprayer gun with 3 bar operating pressure. The loading of the LDO particles in the composite layers were 0, 20, 40, 60, 80 and 100 wt.%, respectively inserted into the low energy fluoropolymer binding material. 10 wt% aqueous suspensions were prepared with varied LDO/fluoropolymer content. The gravimetrically measured specific amount of material deposited on the glass plates was $5.8 \pm 0.1 \text{ mg/cm}^2$ in each case.

The nominal LDO/fluoropolymer ratio did not change significantly (0.46–26.8% difference) during the spray-coating film-forming process (Deák et al., 2016).

2.4. Structural and surface information of the LDO/fluoropolymer composite layers – SAXS measurements

Small-angle X-ray Scattering (SAXS) curves were recorded with a slit-collimated Kratky compact small-angle system (KCEC/3 Anton-Paar KG, Graz, Austria) to obtain structural and surface information about the LDO/fluoropolymer composites. The used calculations were include in the *Supporting Information*.

2.5. Surface morphology and elemental composition – scanning electron microscopy (SEM)

The structure and the morphology of the synthesized hydrophilic LDO particles and LDO/fluoropolymer composite layers were examined by field emission scanning electron microscopy (SEM – Hitachi S-4700 microscope), applying a secondary electron detector and

10 kV acceleration voltage. Röntec EDX detector was used for elemental distribution of Al and F atoms for LDO and PPFDA polymer materials in the LDO/fluoropolymer composite layers. The surface shape and distribution of microorganisms adhered to the composite layers were imaged using a scanning electron microscope (Jeol FEG-SEM 7600F).

2.6. Surface roughness

A mechanical profilometer was used to examine the surface roughness of the LDO/fluoropolymer composite layers (Form Talysurf Series 2 from Taylor Hobson Ltd., Leicester, Great Britain). Roughness and waviness were separated using a 0.25 mm Gaussian cut-off filter. The applied length scale was 2000 μm because this scale is long enough to get appropriate average roughness value about the composites with surface microstructure and roughness.

2.7. Apparent static and dynamic contact angle measurements

The hydrophobicity of the composite layers was determined by water contact angle (θ_w). We used an EasyDrop drop shape analysis device (Krüss GmbH, Hamburg, Germany) with a Peltier temperature chamber and a 0.5 mm diameter syringe steel needle. The tests were carried out at room temperature and under normal atmospheric conditions.

Drelich's protocol was used to calculate the advancing (θ_{adv}) and receding (θ_{rec}) contact angles (Drelich et al., 2013). From the obtained angles the total apparent surface free energy (γ_s^{tot}) of the layers was calculated. Knowing the surface tension of distilled water ($\gamma_1 = 72.1 \text{ mN/m}$ at 25 °C) and its contact angle hysteresis defined as the difference between the advancing and receding contact angles (Chibowski et al., 2003) we calculate γ_s^{tot} :

$$\gamma_s^{tot} = \left(\frac{\gamma_1(1+\cos \theta_{adv})^2}{(2+\cos \theta_{rec}+\cos \theta_{adv})} \right) \quad (1)$$

Contact angle measurements were also used to evaluate the polar and dispersive elements. Overall surface free energy (γ_s^{tot}) and its polar (γ_s^P) and dispersion (γ_s^D) components of the composites with increasing LDO loading were determined from two sets of contact angles (water and glycerin) according to Owens-Wendt-Kaelble equation (Owens and Wendt, 1969).

$$\gamma_1(1 + \cos \theta) = 2[\gamma_1^D \gamma_s^D]^{1/2} + 2[\gamma_1^P \gamma_s^P]^{1/2} \quad (2)$$

where, γ_1 is the surface free energy of the liquid; θ is the contact angle of a liquid against the solid. The dispersion component of the surface free energy for liquid is γ_1^D and for solid is γ_s^D . For a liquid, the polar portion of the surface free energy is γ_1^P , whereas for a solid, it is γ_s^P . The obtained surface free energies values of the test liquids from the literature are given in Fig. S3 as inserted table (Torchinsky and Rosenman, 2009).

The underwater stability of the composite layer with 80 wt.% LDO loading was also determined. During the process the composite layers were submerged under the water for 24 hours. Then, the layers were taken out from the water after different immersion time and the wetting properties were characterized by the sessile drop contact angle (θ_w) measurement. At the end of the experiment the composite layers were re-dried and the contact angle were re-measured.

2.8. Preparation of the bacterial cultures

We used three different standard bacterial strains: *Escherichia coli* (*E. coli*) ATCC 35218, *Pseudomonas aeruginosa* (*P. aeruginosa*) ATCC 27853 and *Staphylococcus aureus* (*S. aureus*) ATCC 25923. The three different strains of bacteria were transferred on nutrient agar and incubated at 37 °C 24 h. To obtain the overnight culture, a single colony of each strain was

transferred from nutrient agar to nutrient broth (Biolife, Italy) and incubated at the same conditions.

2.9. Surface charge measurements

Surface charge of LDO photocatalyst was measured by PCD-04 Particle Charge Detector (Mütek Analytic GmbH, Germany) with manual titration. During the process 10 mL of 1 wt.% LDO suspension was titrated with 0.1 wt.% sodium dodecyl sulphate (SDS) negatively charged surfactant solution. Then, 10 mL of 1 wt.% LDO suspension was titrated with 10^5 CFU/mL *E. coli* bacterial suspension at the same experimental condition like in the bacterial adhesion measurements.

The equimolar amount of surfactant or bacteria CFU was determined to the amount of LDO (meq/g or CFU/g), taking into consideration the amount of the added surfactant or bacteria (at the charge neutralization point where the streaming potential equal to 0 mV).

2.10. Monitoring the bacterial adhesion extent

The method of Bohinc et al. (Bohinc et al., 2014) with modifications was used as follows. 1.33 mL of bacterial overnight cultures ($10^8 - 10^9$ CFU/mL) were transferred into 40 mL of fresh nutrient broth, to obtain the concentration from $10^7 - 10^8$ CFU/mL. The sterile LDO/fluoropolymer composite layer coupons (1 cm × 1 cm) were placed into the Petri dishes and 20 mL of the diluted bacterial culture was added. For negative control we used 20 mL of fresh nutrient broth without bacterial culture for each type of coupons.

The bacterial cells adhered to the composite surfaces immediately after inserting the coupons horizontally in the broth (time 0) and after an 18-hour incubation period at 37 °C in aerobic conditions without shaking. The nutrient broth with bacterial culture was removed after the incubation time. The coupons were rinsed five times with sterile PBS buffer before being stained for 5 minutes at room temperature with 3 mL 0.1 percent (w/v) crystal violet suspension

(Merck, Germany). PBS buffer was used to wash the system five times more. The dye was remobilized from the cells with 400 μ L 96 % ethanol for three minutes. The optical density of the extracted dye was measured at wavelength 620 nm (OD_{620}) by microplate reader Infinite 200[®] PRO, Tecan Austria GmbH.

The number of adhered bacterial cells was investigated with scanning electron microscope (Jeol FEG-SEM 7600F). The adhered bacterial cells on the surfaces were expressed as bacterial cells /cm² determined from several SEM micrographs (Kovačević et al., 2016).

2.11. Fluorescence measurements

P. aeruginosa ATCC 27853 was detected by the fluorescence measurements (Tallósy et al., 2016). During the fluorescence experiments 6 μ L of the dye mixture was added for each mL of bacterial suspension ($1 \times 10^5 - 5 \times 10^5$ CFU/mL). In a two-component formulation, the fluorescence dye was used. Component I (SYTO 9) is able to penetrate the bacterial cell wall and mark the DNA of both living and dead bacteria. Component II (Propidium iodide: PI) is incapable of penetrating a bacterial cell wall which is still intact. It can penetrate only in bacteria with damaged membranes, causing a reduction in the SYTO 9 stain fluorescence. According to the user's guide of the viability kit (LIVE/DEAD[®] BacLight[™] Bacterial Viability kit L7007, Life Technologies, Hungary), the bacteria were grown in nutrient broth (Mueller-Hinton) to late logarithmic phase, then placed on the composite surfaces and exposed to blue LED-light (General Electric's, Hungary, $\lambda_{\max} = 405$ nm) for 0, 60, and 120 minutes.

The viability of the bacteria was evaluated with fluorescence microscope (Leica DM IL LED Fluo). Fluorescence at exc./emi. maxima of about 480/500 nm for SYTO 9 stain (green) and 490/635 nm for PI was used to quantify the reduction of live bacteria after different illumination times of the composite layers (red). Thus, intensities of the green and red emission caused by the live and dead bacteria were recorded. The ratio between the number of red and green coloured bacterial cells on the surface was determined after illumination of LED-light.

2.12. The formation of hydroxyl radicals on LDO/fluoropolymer composite layers

The number of reactive hydroxyl radicals at the solid/liquid interface was calculated using the hydrogen peroxide driven luminol based chemiluminescence reaction (Tallósy et al., 2014a, 2014b, 2016). Results were calculated from the chemiluminescence (CL) data obtained from SiriusL Single Tube luminometer (Berthold Detection Systems, Budapest). According to the measurement protocol 3 mg luminol (Sigma-Aldrich) was diluted in 0.5 mL of sodium hydroxide (0.1 M) and filled out to 10 mL with distilled water. The composite layers (5 cm × 5 cm) were immersed in 40 mL distilled water and illuminated with LED-light (λ_{\max} = 405 nm) and continuously shaken. The distance of the LED-light source from the composite films was 5 cm. Then, 100 μ L samples were taken after 2.5, 5, 10, 15, 20, 30, 40, 50, 60, 75 and 90 minutes of illumination time and were added to 100 μ L of luminol solution of concentration 33.8 mM. The intensity of the CL was measured immediately by the luminometer. The calibration curve was previously determined in the range of 0 - 5 mM of hydrogen peroxide (Fig. S4). The calculated concentration of ROS (expressed as $C_{H_2O_2}$ equivalent) coming from the decomposition of H_2O_2 is directly proportional to the measured relative light unit (RLU/s):

$$C_{H_2O_2} = \frac{(RLU/s)}{41866} \quad (2)$$

where 41866 is the slope of the calibration curve.

From the RLU data, the free radical concentration was computed using $C_{H_2O_2}$ and plotted as a function of illumination time for varying LDO concentrations within the layer.

2.13. Mechanical stability measurements

To evaluate the abrasion resistance of coatings the taber abraser test is frequently used (Rossi et al., 2009). A 418 type manual Taber Abraser was used for the abrasion tests. During the

measurement the composite sample with 80 wt.% LDO content was abraded and the contact angles of the tested surfaces were measured as a function of abrasion cycle.

3. Results and discussion

The purpose of our study was to obtain antibacterial and water-repellent coatings, which have low surface free energy and rough surface structures. This can be obtained with LDO particles embedded into the low energy PPFDA fluoropolymer matrix. We measured the structural, morphological, photocatalytic and bacterial adhesion properties of these composite layers.

3.1. Surface roughness and contact angle determination of the composite layers

The morphological characteristics of LDH are significantly affected by the synthesis conditions. In the presence of urea, spherical LDH can be obtained (Deák et al., 2015). One possible explanation for the formation of spherical LDH is that in a medium containing carbonates, at low pH (pH= 3) and high temperature, the decomposition of urea gives rise to NH_3 and CO_2 gas bubbles, initiating nucleus formation.

After a calcination method, the original Zn content of the special ZnMgAl-LDH (Deák et al., 2016) was converted into photocatalytically active ZnO content layered double oxide (LDO). The ZnO content of LDO was calculated from the Zn content of the initial LDH assuming complete oxidation during the calcination. The original spherical morphology of LDH was still retained and $25.31 \pm 2.34 \mu\text{m}$ spherical LDO particles were obtained (Fig. 1).

Fig. 2 shows the contact angle values of composite layers as a function of surface roughness (R_q). As it can be seen the increase of the LDO content (from 20 wt.% to 80 wt.%) resulted and increase in the R_q values from $0.002 \mu\text{m} \pm 0.0002 \mu\text{m}$ to $15.3 \mu\text{m} \pm 2.04 \mu\text{m}$ and consequently the Θ_w values were also increased from 105.6° to 156.3° . The inset of Fig. 2 shows SEM micrographs of the smooth and rough surfaces. Increasing the LDO content in the composite layers resulted greater surface roughness and contact angle values. 149.1° and 156.3° contact angles were achieved at 60 and 80 wt.% LDO content. This indicates that the superhydrophobic

layers were obtained. Due to the hydrophilic characteristic of LDO particles, a pure LDO layer (without fluoropolymer coating) is superhydrophilic and we were able to achieve a fine, superhydrophilic surface in this manner.

Furthermore, the obtained thickness of the layers were between $64 \pm 1.03 \mu\text{m}$ and $197 \pm 1.80 \mu\text{m}$ (see Fig. S5). The thickness and porosity increases with the increasing LDO content which is also clearly visible from the presented SEM micrographs (Fig. S6). The porosity of films varies between 17.5 and 58.1% (Deák et al., 2016).

The EDX measurements also reveal that the surface of the composite is uniform and the elemental distribution of the Al from LDO and F from PPFDA is in accordance with the LDO loading (Fig. S7).

We consider the mechanical durability of the composite coating because the water repellent superhydrophobic surfaces are highly susceptible to abrasion damage during the service. The angle θ decreases with the aggravated abrasion and it takes a constant value of $\sim 136^\circ$ after 20 cycles (Fig. 3). Even though the coating has lost its superhydrophobicity, the inserted EDX pictures show that the above presented heterogeneous surface structure with simultaneous presence of LDO and fluoropolymer doesn't change.

3.2. Surface energy of LDO/fluoropolymer composite

The surface hydrophobicity of composite layers was characterized by the dynamic contact angle measurement determining the advancing (θ_{adv}) and receding (θ_{rec}) contact angles (Fig. 4). With increasing volume of the water droplet on the pure PPFDA fluoropolymer layer the advancing contact angle (θ_{adv}) decreases from $\theta_{(6.1\mu\text{l})} = 105.6^\circ$ to $\theta_{(49.7\mu\text{l})} = 89.1^\circ$ (Fig. 4). The receding contact angle (θ_{rec}) is progressively decreasing with decreasing volume of the droplet and the final value is significantly lower ($\theta = 24.7^\circ$) than the static contact angle (105.6°). This high contact angle hysteresis ($\Delta\theta_w = 80.9^\circ$) indicates a relatively good wetting properties of the pure fluoropolymer layer. However, in the case of rough superhydrophobic composite layer with 80

wt.% of LDO content, the Θ_{adv} was changed from $\theta_{(7.0\mu l)} = 156.1^\circ$ to $\theta_{(44.6\mu l)} = 150.2^\circ$. The Θ_{rec} changed for smaller amount from 150.2° to 143.7° . The angle hysteresis was $\Delta\theta_w = 12.4^\circ$ which is characteristic for superhydrophobic surfaces (McHale et al., 2004). The total apparent surface free energy γ_s^{tot} calculated from Equation (1) is $28.0 \text{ mJ/m}^2 \pm 3.91 \text{ mJ/m}^2$ for pure polymer whereas for the superhydrophobic composite layer $\gamma_s^{tot} = 2.7 \text{ mJ/m}^2 \pm 0.65 \text{ mJ/m}^2$.

The surface energy demonstrates the differences between the two types of surfaces. The PPFDA polymer with a low surface free energy $\gamma_s^{tot} = 28.0 \text{ mJ/m}^2 \pm 3.91 \text{ mJ/m}^2$ with smooth surface ($R_q = 0.002 \mu\text{m} \pm 0.0002 \mu\text{m}$) was further reduced to $\gamma_s^{tot} = 2.7 \text{ mJ/m}^2 \pm 0.65 \text{ mJ/m}^2$ with the enhanced surface roughness ($R_q = 15.3 \mu\text{m} \pm 2.04 \mu\text{m}$) of the composite layer containing 80 wt.% of LDO. Thus, after the roughening process the hydrophobic layer showed superhydrophobic properties. This reducing tendency of the surface free energy caused by the increasing roughness is presented in Fig. S8. The increased ratio of incorporated LDO particles in the fluoropolymer from 0 to 80 wt.% caused a continuous increase of R_q from $0.002 \mu\text{m} \pm 0.0002 \mu\text{m}$ to $15.3 \mu\text{m} \pm 2.04 \mu\text{m}$ and continuous decrease of γ_s^{tot} from $28.0 \text{ mJ/m}^2 \pm 3.91 \text{ mJ/m}^2$ to $2.7 \text{ mJ/m}^2 \pm 0.65 \text{ mJ/m}^2$.

The total surface free energy (γ_s^{tot}) and its polar (γ_s^P) and dispersion (γ_s^D) components were also determined in accordance with to Owens-Wendt-Kaelble equation (see Fig. S3). Since PPFDA is a chemically inert and hydrophobic fluoropolymer, it has a relatively low γ_s^{tot} ($24.65 \pm 0.56 \text{ mJ/m}^2$) mainly with γ_s^P contribution. Increasing the LDO loading, the γ_s^{tot} values were continuously decreased to $3.39 \pm 0.68 \text{ mJ/m}^2$ (80 wt.% LDO content). Over 80 wt.% LDO loading, the γ_s^{tot} was drastically increased ($62.40 \pm 0.98 \text{ mJ/m}^2$ at 100% LDO content) and the ratio of γ_s^P and γ_s^D values was also changed ($13.77 \pm 0.93 \text{ mJ/m}^2$ and $48.63 \pm 1.04 \text{ mJ/m}^2$) indicating the hydrophilic surface characteristic of the film. This is because over 80% LDO content the surface is mainly covered by hydrophilic LDO (see EDX results in Fig. S7) and the surface turns from hydrophobic to hydrophilic.

3.3. SAXS measurements

The micro surface roughness of the layers was presented in Fig. 2, however, the composite layers also have nanostructural arrangements and inner surface morphology. SAXS scattering curves (Fig. S9) was used to determine the surface roughness and the specific surface area of the LDO/fluoropolymer composite layers on nanoscale.

The $\ln(h^3I)$ vs. h^2 (Porod) plot of the SAXS scattering curves (Fig. S9) was used to determined the surface roughness and the specific surface area of the LDO/fluoropolymer composite layers. The asymptotic behaviour suggests a flat surface for 40 wt.% LDO containing composite layer (see Fig. S9). With the increasing LDO content, a positive deviation can be observed caused by the increasing surface roughness of the composite layers (Fig. S9). The Porod constant can be determined by the intercept of the fit, which constant is suitable for calculating the specific surface area (a^s) of the samples. The a^s value obtained by SAXS method presented in Table 1 is increasing with the increasing LDO content. For the 40 wt.% LDO content, the obtained surface fractal dimension (D_s) was 2 which value related for a smooth surface. When the particle content is increasing in the composite layer a higher value (2.1-2.25 for 80 wt.% and 100 wt.% LDO) was obtained for the D_s (Table 1). The scattering curves of the 40-100 wt.% LDO/fluoropolymer layers presented in Fig. 5(a) shows a characteristic peak appeared at $h=2.66 \text{ nm}^{-1}$, which, based on calculations using the $D=2\pi/h$ (D : diameter in nm) relationship, is indicative of the formation of scattering centers with a characteristic size of $D=2.36 \text{ nm}$. This is assumed to be the consequence of the LDO particles in the composite layer. With the increasing LDO content less particles will be covered with fluoropolymer and surface become more roughed. This is also confirmed by the analysis of the log-log plot (Fig. 5(b)). The surface roughness and the tail end constant (K_p) were systematically increased from 0.2 to 1.54 and from 2 to 2.25 (Table. 1).

Here the obtained values for the surface were in nano dimension which refer more to the nanostructural property of the layers.

3.4. Determination of microbial adhesion capacity on the surface of composite layers

The literature data confirms our observations that with the increasing surface micro- roughness the bacterial adhesion extent to the surface increases (Taylor et al., 1998; Diaz et al., 2007; Lorenzetti et al., 2015; Zhang et al., 2013; Katsikogianni and Missirlis, 2004). Fig. 6 presents the adhesion extent of three bacterial strains on composite layers as a function of increasing LDO particle content. The optical density OD_{620} of crystal violet dye indicates that the adhesion capacity of all bacterial strains strongly depends on surface characteristics. The increasing surface roughness increases OD_{620} .

The inset of Fig. 6 shows two photos of the crystal violet coloured films. From photos we conclude that the bacterial adhesion on the relatively smooth surface of fluoropolymer (with 0 wt.% of LDO particles) was the least pronounced. This type of surface was colourless, which means that all three types of bacterial cells are not or only slightly adhered to the surface (after 18 h of incubation time at 37 °C under aerobic conditions). The measured OD_{620} value of the extracted dye was between 0.01 and 0.05 (1.19×10^5 cells/cm² and 5.39×10^5 cells/cm², Fig. S10). The determined OD_{620} was the highest ($OD_{620} = 1.11-1.54$) in the case of the most rough surface ($R_q = 15.3 \mu\text{m} \pm 2.04 \mu\text{m}$) with 80 wt.% of LDO content. The layer was coloured blue, and shows the presence of bacterial cells on the surface (inset of Fig. 6). The control measurements (without 18 h of bacterial incubation) indicate that the crystal violet dye do not colour the composite surface, from which follows that only the adhered bacteria were coloured. We note that according to these microbial adhesion capacity measurements the presence of bacterial cells on the composite surface increases with the increasing LDO content and the highest bacterial adhesion was measured just for the superhydrophobic ($\theta = 156.3^\circ$), 80 wt.% LDO containing sample. The adhered cell numbers for *P. aeruginosa*, *E. coli* and *S. aureus*

were 1.58×10^7 , 1.47×10^7 and 1.20×10^7 cells/cm², respectively (Fig. S10). The reason for the bacterial adhesion is the decreased coatings superhydrophobicity after immersion in water. The underwater metastability of superhydrophobic surfaces is due to three main physical mechanisms: pressurization, air diffusion, and droplet condensation. These physical mechanisms induce the wetting transition on water submerged superhydrophobic surfaces (Marmur, 2006; Cheng et al., 2019; Xue et al., 2016). Fig. S11 presents the effect of immersion time duration on the measured contact angles of superhydrophobic coating. Initially superhydrophobic surface ($\theta = 156.3^\circ$) lost their non-wetting characteristic under a relatively short period of time (120 min). However, the layers didn't lose their antibacterial properties (see subsection 3.7). The re-dried coating has shown superhydrophobic properties again indicating the reversible nature of the process.

The results of the underwater experiments allow to conclude that the bacterial adhesion increases with the LDO loading which is due to the greater bacterial attraction on the free, uncovered LDO parts rather than the greater retention against washing/rinsing process during the experiment.

3.5. Scanning electron microscopy

The bacterial adhesion was also investigated by SEM micrographs. Fig. 7 shows a representative SEM micrographs of 80 wt.% LDO containing composite layer without (Fig. 7(a)) and with (Fig. 7(b)) adhered *S. aureus* bacteria. At this high LDO content the low energy fluoropolymer does not completely cover the surface of the LDO particles. Isolated polymer islands can be observed in Fig. 7(a) and it can be seen that the *S. aureus* bacteria obviously preferred the high energy LDO surfaces instead of the low energy polymer (Fig. 7(b)). Our results are in agreement with the literature data of Li and Logan (Li and Logan, 2004) who reported that the presence of different metal-oxides (e.g. TiO₂, SnO₂, Al₂O₃, Fe₂O₃, etc.) can increase the bacterial adhesion. Their explanation was that the negatively-charged bacteria

prefer to adhere to positively charged oxide surfaces. It was confirmed that the bacteria have an attractive electrostatic contact with the positively charged LDO particles. The surface charge density of the LDO particles was estimated from the streaming potential data. 10 mL 1 wt.% LDO suspensions was titrated with 0.1 wt.% SDS negatively charged surfactant solution (Fig. 8(a)). The LDO suspension was positive and during the addition of oppositely charged SDS the streaming potential continuously decreases. Taking into account the added amount of surfactant molecules ($n_{\text{SDS}} = 0.0028 \text{ mmol}$) for the charge compensation of LDO and the mass of the titrated LDO ($= 0.1 \text{ g}$), the specific surface charge of LDO was equal to $+0.028 \text{ meq/g}$. The streaming potential of 10 mL 1 wt.% positively charged LDO suspension was also titrated with 10^5 CFU/mL *E. coli* bacterial suspension (Fig. 8(b)) at the same experimental condition (fresh nutrient broth solution with given pH and ionic strength). Positive streaming capacity ($+509 \text{ mV}$) is present in the initial LDO suspension, but it decreases as the number of negatively charged bacteria increases. According to the obtained electrostatic charge compensation point (0 mV streaming potential at 0.14 mL 10^5 CFU/mL *E. coli* bacteria suspension consumed), $1.4 \times 10^5 \text{ CFU}$ *E. coli* bacteria is electrostatically adhered to 1 g LDO particles. These results confirm that the bacterial adhesion extent depends also on the electrostatic interactions between LDO and bacterial cells ($5 \times 10^6 \text{ CFU/meq}$).

In the Wenzel's model, the hydrophilicity/hydrophobicity of a homogeneous substrate is amplified by decreasing/increasing surface roughness (Khan and Singh, 2013). The presented EDX measurements (Fig. S7) revealed that the coating shows superhydrophobic properties for 80 wt.% LDO content. The surface of films is heterogeneous, beside the fluoropolymer parts there are also regions of LDO particles which are not covered with a polymer. Fig. 9 presents SEM micrographs of the surface with 80 wt.% of LDO content with adhered *P. aeruginosa* (Fig. 9 a/1 and a/2), *E. coli* (Fig. 9 b/1 and b/2) and *S. aureus* (Fig. 9 c/1 and c/2) after 18 h incubation time. It can be seen that most of bacterial cells are adhered on the surface of LDO

particles (Fig. 9 a/1, b/1 and c/1). More precisely, the bacteria are adhered to the lamellae, voids and gaps of LDO particles (Fig. 9 a/2, b/2 and c/2).

3.6. Determination of reactive radicals on photoreactive composite layers

At higher LDO content the polymer coverage is not complete and accessible LDO particles can be found on the surface of composite layers. Moreover, the LDO with app. 12 wt.% ZnO content shows photocatalytic activity according to the benzoic acid photodegradation tests presented in our previous paper (Deák et al., 2016).

During the photocatalytic process reactive oxygen species (ROS) were produced, which are primarily responsible for bacterial inactivation and cause an irreversible DNA degradation in bacterial cells (Block, 2001). To detect these radicals in the presence of luminol the chemiluminescence method has been used (Min et al., 2007).

The photocatalytically generated radicals (ROS) react with luminol, produce chemiluminescence (CL) and the concentration of ROS is correlated with the amount of photoluminescence photons (Fig. S12) (Schneider, 1970). The degradation of the formed hydrogen peroxide is slow at room temperature and is measured with a luminometer (Perez-Benito, 2004). In this way the concentration of H_2O_2 is proportional to the difference of free radicals produced under appropriate illumination and consequently the ROS concentration can be expressed as equivalent H_2O_2 (mM) concentration. The equivalent concentration values of H_2O_2 (mM) as a function of illumination time is shown in Fig. 10 and exhibit an increase of producing radicals as a function of increasing illumination time. All curves saturates at larger illumination time. In the case of 80 wt.% LDO/fluoropolymer layer the amount of the ROS OH^\cdot is higher (0.34 mM H_2O_2 equivalent) than in the presence of lower LDO content composite layers (0.27; 0.19 and 0.12 mM H_2O_2 equivalent at 60, 40 and 20 wt.% LDO content) after 90 minutes of LED-light illumination. The observed saturation of the curves is the result of the undesired partial photo-degradation of the polymer binder (Veres et al., 2014). The long-term

illumination impact the composition of catalyst/polymer as the photocatalyst particles became uncoated (Janovák et al., 2017) and this also caused the continuous decreasing of the measured contact angle values (Lantos et al., 2020).

In our previous works we studied the effect and durability of polymer binder on photocatalytic and structural properties (Veres et al., 2014). During these tests the nanocomposites were exposed to photoaging, which resulted in a notable increase of the photocatalytic activity, due to the partial photooxidation of polymer matrix on the surface which resulted better availability for surface photocatalyst to the model pollutant. We found that after 24 h of photoaging, the nanocomposites could perform similarly to the pure catalysts, but the mechanical stability was heavily decreased (Veres et al., 2014). Therefore, to reduce the photodegradation of the polymer binder we applied more inert hydrophobic fluoropolymers (e.g. perfluorinated polyacrylates like poly(perfluorodecyl acrylate) (PPFDA)) as a binder material.

The above presented microbial adhesion capacity measurements show that all three types of bacterial cells are preferentially adhered to the surface of LDO photocatalyst particles which is advantageous from the viewpoint of long term- use. Namely, it is well known that the photocatalytic surfaces with generated free radicals are suitable for the continuous bacterial inactivation and inhibition of biofilm formation (Sirelkhatim et al., 2015; Achouri et al., 2018).

3.7. Bacterial cell inactivation measured by fluorescence microscopy

The LDO particles displayed photocatalytic properties (due to app. 12 wt.% of ZnO content) under LED-light illumination and produced reactive ROS. The inactivation of bacterial cells on the 80 wt.% LDO containing superhydrophobic composite layers were investigated by fluorescence microscopy. The bacterial suspension of *P. aeruginosa* was stained with Bacterial Viability staining kit and examined at the beginning of the experiment ($t=0$ min), after 1 and 2 hours of illumination with LED-light source. Fig. 11 presents the fluorescence microscopy

images with the regions of the live (green) and damaged (red) *P. aeruginosa* cells on the 80 wt.% LDO containing composite layer.

At the beginning ($t = 0$ min) all bacterial cells have green emission (by SYTO 9). After 120 min of illumination part of bacterial cells are damaged. Therefore, the intensity of green emission is significantly reduced due to the cell wall penetrating PI into the damaged bacterial cell wall (Fig. 11). In parallel, at the same initial time ($t = 0$ min) negligible (1-2) damaged (or dead) bacterial cells were observed. The number of damaged (red emission) cells increased after 120 minutes of light exposure (Fig. 11). The percentage of live and damaged *P. aeruginosa* bacterial cells was calculated from the fluorescence microscopy images and presented in Fig. 12. The number of live bacterial cells after 120 min of illumination was reduced by 93%. At this time, the number of damaged bacterial cells increased to 46%. The obtained bacterial inactivation is due to the generated free radicals and the photocatalysis is important in the inactivation of bacteria instead of the direct photolysis (Tallósy et al., 2016).

The fluorescent dye kit consists of two components, SYTO 9 (green) dye and propidium iodide fluorescent dye (PI, red). The SYTO 9 dye enters in both living and damaged bacterial cells, but PI dye cannot penetrate in the living bacterial cells, only if the cell wall is damaged. Although both fluorescent dyes stain the damaged cells, when used together, propidium iodide reduces the intensity of green dye emission (extinguishes) so that only the red color is visible (Tallósy et al., 2016). As a result, the use of a dye kit is excellent for the combined detection of intact (LIVE) and damaged (DEAD) cells. During photocatalytic inactivation, the wall of bacterial cells is damaged and significant degradation occurs in their peptidoglycan layer. This large extent of damage does not always allow the stained parts to be similarly visible as cells that have survived or are initially damaged.

4. Conclusion

Within this study, we develop a novel antibacterial coating composed of photoreactive LDO particles embedded in a low surface energy fluoropolymer matrix.

The surface roughness, charge, wettability and bacterial adhesion properties can be varied by adjusting the loading of LDO particles into the fluoropolymer matrix. The increasing LDO content (from 0 to 80 wt.%) increases of the surface roughness (from $0.002\ \mu\text{m} \pm 0.0002\ \mu\text{m}$ to $15.3\ \mu\text{m} \pm 2.04\ \mu\text{m}$). The composite layer (with 80 wt.% LDO content) has shown superhydrophobic and water-repellent properties with high contact angle ($156.1^\circ \pm 2.56^\circ$) and low surface free energy ($2.7\ \text{mJ/m}^2 \pm 0.65\ \text{mJ/m}^2$). On these composite layers we studied bacterial adhesion of *S. aureus*, *E. coli* and *P. aeruginosa*. We observed that the adhesion extent increases with increasing roughness of the surface layers. The reason for pronounced bacterial adhesion is the electrostatic attraction between LDO particles and bacterial cells as well as attraction between hydrophilic LDO particles and hydrophilic bacteria. The SEM micrographs confirmed that bacteria preferably adhered to the lamellae of LDO surfaces. Due to 12 wt.% nominal content of ZnO phase in LDO particles, the composite layer has a photocatalytic property. To LDO particles adhered bacteria were photocatalytically inactivated by illuminating with LED-light for 120 min. The number of live bacteria decreases to zero with increasing illumination time.

The presence of different metal-oxides increase the bacterial adhesion since the bacteria with negative charge prefer to adhere to positively charged oxide surfaces. However, this conventional metal surfaces show very hydrophilic even superhydrophilic properties. In the case of our non-conventional composite layers with heterogeneous surface energy distribution, controllable wetting and photocatalytic properties are achieved. The bacterial adhesion preferably occurred on the lamellae of LDO photocatalyst surfaces. These composite layers can be optimized to the maximal bacterial adhesion extent. Consequently, the extent of inactivated bacteria could be maximized and ready for the inactivation with LED-light illumination. The developed composite layers can have an important application in photocatalytic air purifying

and sterilizing systems and are very good for health care facilities with surfaces of antiseptic and disinfectant properties. Moreover, the performed composite layer with controllable bacterial adhesion and obvious photoreactive properties is potentially useful in the area of waste water treatment, as well.

Conflicts of interest

There are no declared conflicts.

Acknowledgements.

The authors are grateful for the financial assistance from the National Research, Development and Innovation Office (GINOP-2.3.2-15-2016-00013 and GINOP-2.1.7-15-2016-01987) and from the COST Action STSM CM1101. This paper was also supported by the UNKP-22-5 and UNKP-21-4 New National Excellence Program of the Ministry for Innovation and Technology from the source of the National Research, Development and Innovation Fund and by the János Bolyai Research Scholarship of the Hungarian Academy of Sciences. KB and KGT are very thankful for the Slovenian Research Agency for support through program P3-0388. All these supports are highly appreciated.

References

- Achouri, F., Merlin, C., Corbel, S., Alem, H., Mathieu, L., Balan, L., Medjahdi, G., Said, M. B., Ghrabi, A., Schneider, R., 2018. ZnO Nanorods with High Photocatalytic and Antibacterial Activity under Solar Light Irradiation. *Materials* 11(11), 2158.
- Bayoudh, S., Othmane, A., Ponsonnet, L., Ouada, H. B., 2008. Electrical detection and characterization of bacterial adhesion using electrochemical impedance spectroscopy-based flow chamber. *Colloids Surf. A: Physicochem. Eng. Asp.* 318, 291-300.
- Block, S. S., 2001. Disinfection, sterilization and preservation, fifth ed., Lippincott Williams & Wilkins, Philadelphia, USA.
- Bohinc, K., Dražič, G., Fink, R., Oder, M., Jevšnik, M., Nipič, D., Godič Torkar, K., Raspor, P., 2014. Metal surface characteristics dictate bacterial adhesion capacity. *Int. J. Adhes. Adhes.* 50, 265–272.
- Bohinc, K., Dražič, G., Abram, A., Jevšnik, M., Jeršek, B., Nipič, D., Kurinčič, M., Raspor, P., 2016. Available surface dictates microbial adhesion capacity. *Int. J. Adhes. Adhes.* 68, 39–46.
- Bos, R., van der Mei, H. C., Busscher, H. J., 1999. Physico-chemistry of initial microbial adhesive interactions - Its mechanisms and methods for study. *FEMS Microbiol. Rev.* 23, 179–230.
- Carja, G., Kameshima, Y., Nakajima, A., Dranca, C., Okada, K., 2009. Nanosized silver–anionic clay matrix as nanostructured ensembles with antimicrobial activity. *Int. J. Antimicrob. Agents* 34(6), 534-539.
- Chen, B., Qiu, J., Sakai, E., Kanazawa, N., Liang, R., Feng, H., 2016. Robust and superhydrophobic surface modification by a “paint+adhesive” method: applications in self-cleaning after oil contamination and oil-water separation. *ACS Appl. Mater. Interfaces*, 8(27), 17659–17667.
- Cheng, Y., Feng, G., Moraru, C. I., 2019. Micro- and Nanotopography Sensitive Bacterial Attachment Mechanisms: A Review. *Front. Microbiol.* 10, 191-208.

Chibowski, E., 2003. Surface free energy of a solid from contact angle hysteresis. *Adv. Colloid Interface Sci.* 103, 149–172.

Chung, C.-J., Lin, H.-I., Tsou, H.-K., Shi, Z.-Y., He, J.-L., 2008. An antimicrobial TiO₂ coating for reducing hospital-acquired infection. *J. Biomed. Mater. Res. Part B Appl. Biomater.* 85B(1), 220–224.

Deák, Á., Janovák, L., Tallósy, Sz. P., Bitó, T., Sebők, D., Buzás, N., Pálínkó, I., Dékány, I. (2015). Spherical LDH–Ag⁺-Montmorillonite Heterocoagulated System with a pH-Dependent Sol–Gel Structure for Controlled Accessibility of AgNPs Immobilized on the Clay Lamellae. *Langmuir*, 31(6), 2019–2027.

Deák, Á., Janovák, L., Csapó, E., Ungor, D., Pálínkó, I., Puskás, S., Ördög, T., Ricza, T., Dékány, I., 2016. Layered double oxide (LDO) particle containing photoreactive hybridlayers with tunable superhydrophobic and photocatalytic properties. *Appl. Surf. Sci.* 389, 294–302.

Diaz, C., Schilardi, P. L., Salvarezza, R. C., Fernández Lorenzo de Mele, M., 2007. Nano/Microscale Order Affects the Early Stages of Biofilm Formation on Metal Surfaces, *Langmuir* 23, 11206-11210.

Drelich, J., 2013. Guidelines to measurements of reproducible contact angles using a sessile-drop technique. *Surf Innov.* 1(4), 248-254.

Dunne, C. P., Keinänen-Toivola, M. M., Kahru, A., Teunissen, B., Olmez, H., Gouveia, I., Melo, L., Murzyn, K., Modic, M., Ahonen, M., Askew, P., Papadopoulos, T., Adlhart, C., Crijns, F. R. L., 2017. Anti-microbial coating innovations to prevent infectious diseases (AMiCI): Cost action ca15114. *Bioengineered* 8:6, 679-685.

Dunne, S. S., Ahonen, M., Modic, M., Crijns, F. R. L., Keinänen-Toivola, M. M., Meinke, R., Keevil, C. W., Gray, J., O’Connell, N. H., Dunne, C. P., 2018. Specialized cleaning associated with antimicrobial coatings for reduction of hospital-acquired infection: opinion of the COST Action Network AMiCI (CA15114). *J. Hosp. Infect.* 99, 250-255.

- Fateh, R., Dillert, R., Bahnemann, D., 2014. Self-Cleaning Properties, Mechanical Stability, and Adhesion Strength of Transparent Photocatalytic TiO₂–ZnO Coatings on Polycarbonate. *ACS Appl. Mater. Interfaces* 6(4), 2270–2278.
- Fresno, F., Portela, R., Suárez, S., Coronado, J. M., 2014. Photocatalytic materials: recent achievements and near future trends. *J. Mater. Chem. A* 2, 2863–2884.
- Fujishima, A., Honda, K., 1972. Electrochemical photolysis of water at a semiconductor electrode. *Nature* 238, 37–38.
- Ghosh, R., Swart, O., Westgate, S., Miller, B. L., Yates, M. Z., 2019. Antibacterial copper-hydroxyapatite composite coatings via electrochemical synthesis. *Langmuir* 35(17), 5957–5966.
- Hasan, J., Raj, S., Yadav, L., Chatterjee, K., 2015. Engineering a Nanostructured “Super Surface” with Superhydrophobic and Superkilling Properties. *RSC Adv.* 5 (56), 44953–44959.
- Herrald, P. J., Zootolla, E. A., 1988. Scanning electron microscopic examination of *Yersinia enterocolitica* attached to stainless steel at elevated temperature and pH values. *J. Food Sci.* 51, 445–448.
- Janovák, L., Deák, Á., Tallósy, Sz. P., Sebők, D., Csapó, E., Bohinc, K., Abram, A., Pálinkó, I., Dékány, I., 2017. Hydroxyapatite-enhanced structural, photocatalytic and antibacterial properties of photoreactive TiO₂/HAp/polyacrylate hybrid thin films. *Surf. Coat. Technol.* 326, 316–326.
- Katsikogianni, M., Missirlis, Y. F., 2004. Concise review of mechanisms of bacterial adhesion to biomaterials and of techniques used in estimating bacteriamaterial interactions. *Eur Cell Mater* 8, 37–57.
- Khan, S., Singh, J. K., 2013. Wetting transition of nanodroplets of water on textured surfaces: a molecular dynamics study. *Mol Simul.* 40(6), 458–468.

- Kovačević, D., Pratnekar, R., Godič Torkar, K., Salopek, J., Dražić, G., Abram, A., Bohinc, K., 2016. Influence of Polyelectrolyte Multilayer Properties on Bacterial Adhesion Capacity. *Polymers* 8(10), 345.
- Lantos, E., Mérai, L., Deák, Á., Gómez-Pérez, J., Sebők, D., Dékány, I., Kónya, Z., Janovák, L., 2020. Preparation of sulfur hydrophobized plasmonic photocatalyst towards durable superhydrophobic coating material. *J Mater Sci Technol*, 41, 159–167.
- Li, B., Logan, B. E., 2004. Bacterial adhesion to glass and metal-oxide surfaces. *Colloids Surf. B* 36, 81–90.
- Li, R., Boudot, M., Boissière, C., Grosso, D., Faustini, M., 2017. Suppressing Structural Colors of Photocatalytic Optical Coatings on Glass: The Critical Role of SiO₂. *ACS Appl. Mater. Interfaces*, 9(16), 14093-14102.
- Li, Y., Wu, S., Wu, J., Hu, Q., Zhou, C., 2020. Photothermocatalysis for efficient abatement of CO and VOCs. *J. Mater. Chem. A* 8, 8171-8194.
- Liu, K., Jiang, L., 2011. Metallic surfaces with special wettability. *Nanoscale* 3, 825-838.
- Lorenzetti, M., Dogša, I., Stošicki, T., Stopar, D., Kalin, M., Kobe, S., Novak, S., 2015. The Influence of Surface Modification on Bacterial Adhesion to Titanium-Based Substrates. *ACS Appl. Mater. Interfaces* 7, 1644-1651.
- Marmur, A., 2006. Underwater Superhydrophobicity: Theoretical Feasibility. *Langmuir* 24, 1400–1402.
- McHale, G., Shirtcliffe, N. J., Newton, M. I., 2004. Contact-Angle Hysteresis on Super-Hydrophobic Surfaces. *Langmuir*, 10146-10149.
- Min, L., Wu, X.-Z., Tetsuya, S., Inoue, H., 2007. Time-resolved chemiluminescence study of the TiO₂ photocatalytic reaction and its induced active oxygen species. *Luminescence* 22, 105–112.
- Nosonovsky, M., Bhushan, B., 2009. Superhydrophobic Surfaces and Emerging Applications: Non-Adhesion, Energy, Green Engineering. *Curr. Opin. Colloid Interface Sci.* 14 (4), 270–280.

Owens, D. K., Wendt, R. C., 1969. Estimation of the surface free energy of polymers. *J. Appl. Polym. Sci.* 13(8), 1741–1747.

Perez-Benito, J. F., 2004. Iron(III)-hydrogen peroxide reaction: kinetic evidence of a hydroxylmediated chain mechanism. *J. Phys. Chem. A* 108, 4853–4858.

Raghunath A., Perumal, E., 2017. Metal oxide nanoparticles as antimicrobial agents: a promise for the future. *Int. J. Antimicrob. Agents* 49(2), 137-152.

Rossi, S., Deflorian, F., Scrinzi, E., 2009. Reduction of aesthetical properties of organic coatings caused by mechanical damage. *Mater. Des.* 30, 1511–1517.

Saxena, N., Naik, T., Paria, S., 2017. Organization of SiO₂ and TiO₂ Nanoparticles into Fractal Patterns on Glass Surface for the Generation of Superhydrophilicity. *J. Phys. Chem. C* 121(4), 2428–2436.

Schneider, H. W., 1970. A new, long-lasting luminol chemiluminescent cold light. *Journal of Chemical Education*, 47(7), 519–522.

Sedelnikova, M. B., Komarova, E. G., Sharkeev, Y. P., Ugodchikova, A. V., Tolkacheva, T. V., Rau, J. V., Buyko, E. E., Ivanov, V. V., Sheikin, V. V., 2019. Modification of titanium surface via Ag-, Sr- and Si-containing micro-arc calcium phosphate coating. *Bioactive Materials* 4, 224–235.

Selim, M. S., El-Safty, S. A., Shenashen, M. A., Higazy, S. A., Elmarakbic, A., 2020. Progress in biomimetic leverages for marine antifouling using nanocomposite coatings. *J. Mater. Chem. B* 8, 3701-3732.

Sirelkhatim, A., Mahmud, S., Seeni, A., Kaus, N. H. M., Ann, L. C., Bakhori, S. K. M., Hasan, H., Mohamad, D., 2015. Review on Zinc Oxide Nanoparticles: Antibacterial Activity and Toxicity Mechanism. *Nano-Micro Lett* 7(3), 219–242.

Tallósy, S. P., Janovák, L., Nagy, E., Deák, Á., Juhász, Á., Csapó, E., Buzás, N., Dékány, I., 2016. Adhesion and inactivation of Gram-negative and Gram-positive bacteria on photoreactive TiO₂/polymer and Ag–TiO₂/polymer nanohybrid films. *Appl. Surf. Sci.* 371, 139–150.

- Tallósy, Sz. P., Janovák, L., Ménesi, J., Nagy, E., Juhász, Á., Balázs, L., Deme, I., Buzás N., Dékány, I., 2014a. Investigation of the antibacterial effects of silver modified TiO₂ and ZnO plasmonic photocatalysts embedded in polymer thin films. *Environ. Sci. Pollut. Res.* 21(19), 11155-11167.
- Tallósy, Sz. P., Janovák, L., Ménesi, J., Nagy, E., Juhász, Á., Dékány, I., 2014b. LED-light Activated Antibacterial Surfaces Using Silver-modified TiO₂ Embedded in Polymer Matrix. *J. Adv. Oxid. Technol.* 17, 9-16.
- Taylor, R. L., Verran, J., Lees, G. C., Ward, A. J. P., 1998. The influence of substratum topography on bacterial adhesion to polymethyl methacrylate. *J. Mater. Sci. Mater. Med.* 9, 17-22.
- Torchinsky, I., Rosenman, G., 2009. Wettability Modification of Nanomaterials by Low-Energy Electron Flux. *Nanoscale Res. Lett.* 4(10), 1209–1217.
- Tung, W. S., Daoud, W. A., 2009. Photocatalytic self-cleaning keratins: A feasibility study. *Acta Biomaterialia*, 5(4), 50-56.
- Tung, W. S., Daoud, W. A., 2011. Self-cleaning fibers *via* nanotechnology: a virtual reality. *J. Mater. Chem.* 21, 7858.
- Veres, Á., Ménesi, J., Juhász, Á., Berkesi, O., Ábrahám, N., Bohus, G., Oszkó, A., Pótári, G., Buzás, N., Janovák, L., Dékány, I., 2014. Photocatalytic performance of silver-modified TiO₂ embedded in poly(ethyl-acrylate-co-methyl metacrylate) matrix. *Colloid. Polym. Sci.* 292, 207–217.
- Veres, Á., Rica, T., Janovák, L., Dömök, M., Buzás, N., Zöllmer, V., Seemann, T., Richardt, A., Dékány, I., 2012. Silver and gold modified plasmonic TiO₂ hybrid films for photocatalytic decomposition of ethanol under visible light. *Catal. Today* 181, 156– 162.
- Xie, X., Mao, C., Liu, X., Tan, L., Cui, Z., Yang, X., Zhu, S., Li, Z., Yuan, X., Zheng, Y., Yeung, K. W. K., Chu, P. K., Wu, S., 2018. Tuning the Bandgap of Photo-Sensitive

Polydopamine/Ag₃PO₄/Graphene Oxide Coating for Rapid, Noninvasive Disinfection of Implants. ACS Cent. Sci. 4(6), 724–738.

Xue, C.-H., Li, M., Guo, X.-J., Li, X., An, Q.-F., Jia, S.-T., 2017. Fabrication of superhydrophobic textiles with high water pressure resistance. Surf. Coat. Technol. 310, 134-142.

Xue, Y., Lv, P., Lin, H., Duan, H., 2016. Underwater Superhydrophobicity: Stability, Design and Regulation, and Applications. App Mech Rev 68(3), 030803.

Zhang, X., Wang, L., Levänen, E., 2013. Superhydrophobic surfaces for the reduction of bacterial adhesion. RSC Adv. 3, 12003-12020.

Zhang, Z., Chen, B., Lu, B., Wu, H., Wu, H., Jiang, S., Chai, G., 2017. A novel thermo-mechanical anti-icing/de-icing system using bi-stable laminate composite structures with superhydrophobic surface. Compos. Struct. 180, 933-943.

Zhu, J., Uliana, A., Wang, J., Yuan, S., Li, J., Tian, M., Simoens, K., Volodin, A., Lin, J., Bernaerts, K., Zhang, Y., Van der Bruggen, B., 2016. Elevated salt transport of antimicrobial loose nanofiltration membranes enabled by copper nanoparticles *via* fast bioinspired deposition. J. Mater. Chem. A 4(34), 13211–13222.

Zisman, W. A., 1964. Relation of the equilibrium contact angle to liquid and solid construction, Adv. Chem. Ser. 43 (1964) 1-51.

Figures

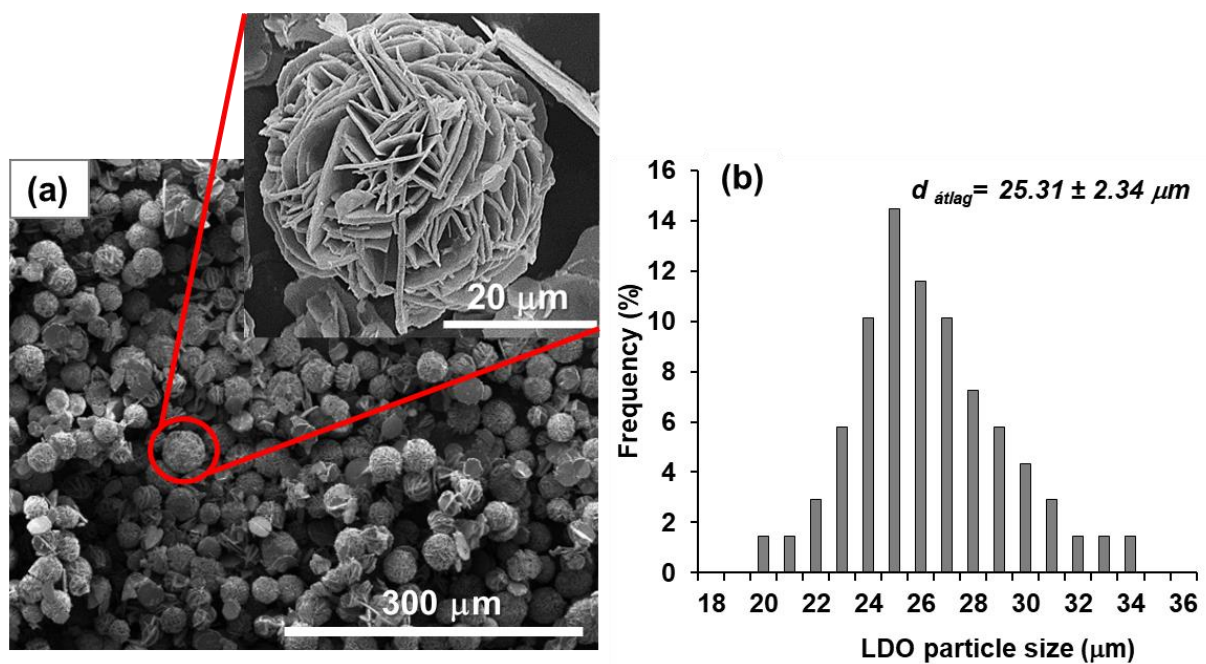


Fig. 1. SEM micrograph (a) and the corresponding size distribution (b) of the LDO photocatalyst particles used for the roughening of the composites.

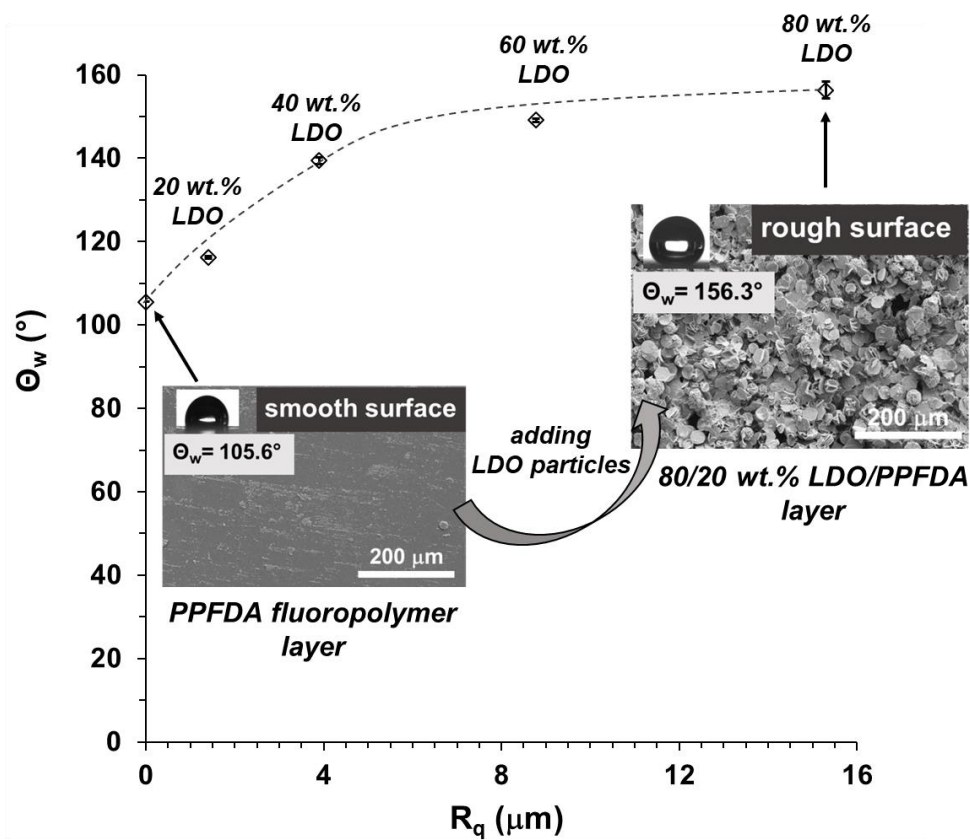


Fig 2. The contact angle values (Θ_w) of composite layers as a function of surface roughness (R_q), ($T = 25\text{ }^\circ\text{C} \pm 0.5\text{ }^\circ\text{C}$). Inset: topographies of surfaces with extreme roughness (rough and smooth) with their water contact angle (Θ_w) values and photographs of the liquid droplets on the composite layers. Smooth surface is composed of only fluoropolymer (PPFDA). Rough surface is composed of 80 wt.% LDO and 20 wt.% PPFDA.

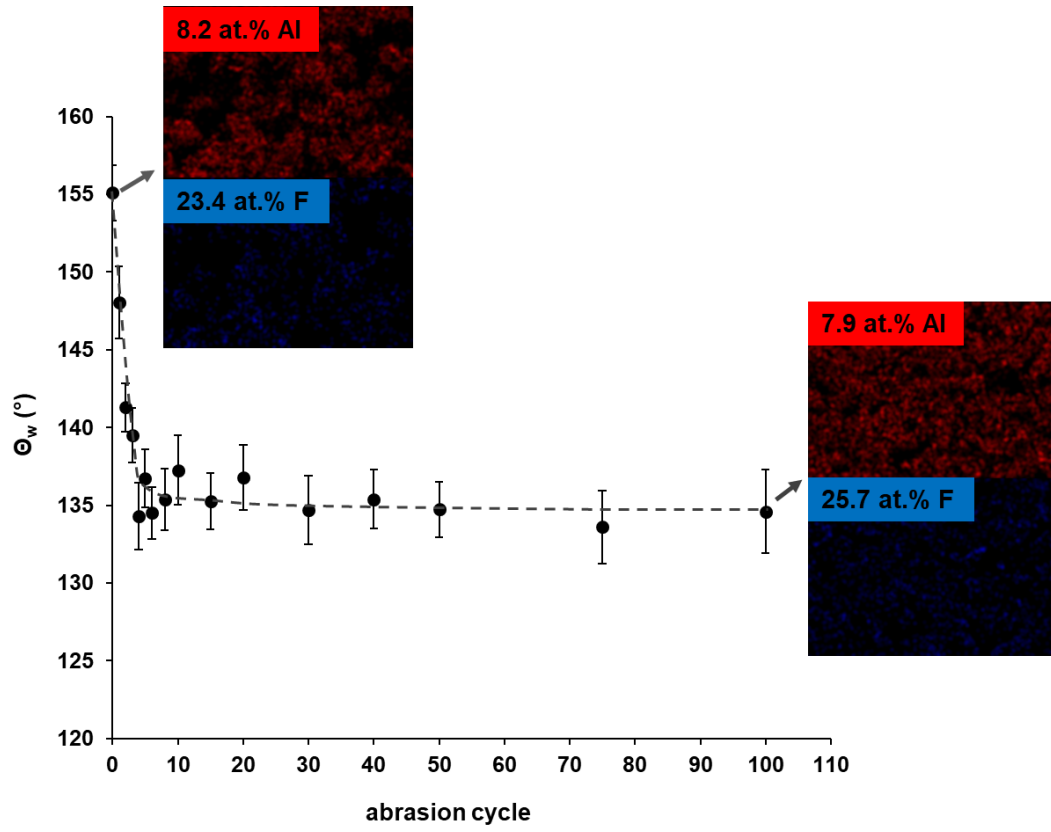


Fig. 3. θ_w as a function of abrasion cycle applied on composite layer composed of 80 wt.% LDO. Inset: the element distribution for Al (red) and F (blue) for the initial composite layer and after 100 abrasion cycles. The dashed line is a guide to eyes.

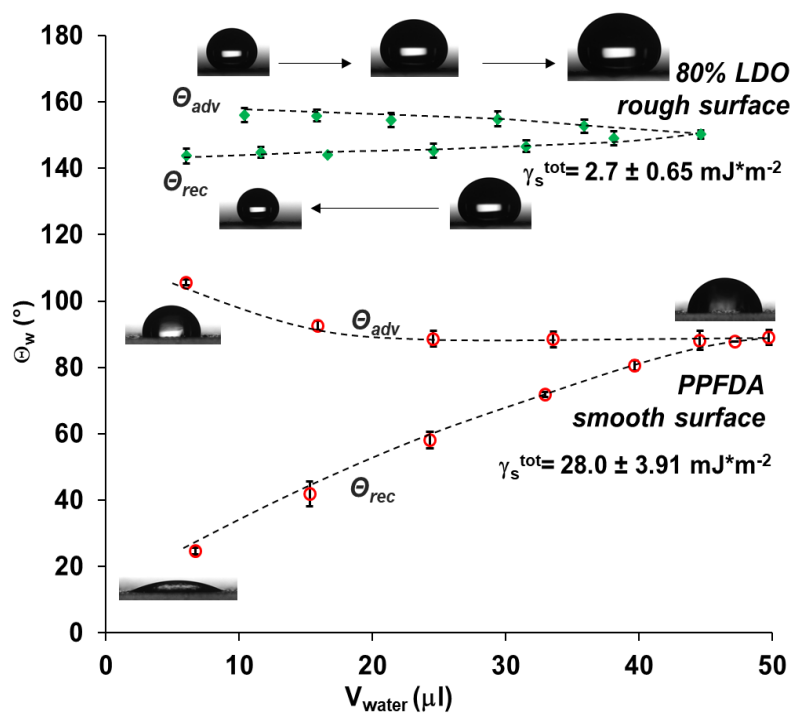


Fig. 4. Advancing (θ_{adv}) and receding (θ_{rec}) water contact angles (θ_w) as a function of water droplet volume (V_{water}) for smooth PPFDA fluoropolymer surface (red) and LDO roughened (80 wt.% LDO) layers (green). The photos of the liquid droplet and on the composite layers and the surface free energy (γ_s^{tot}) values are also presented.

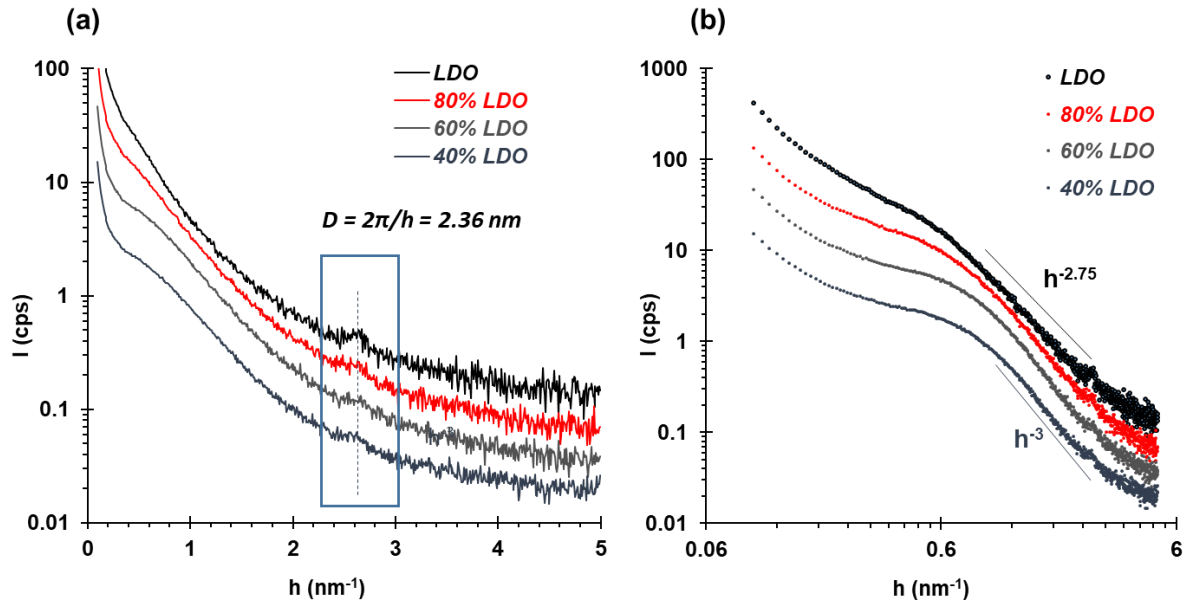


Fig 5. SAXS curves (a) and log-log plot representation (b) of the composite layers with 40, 60, 80 and 100 wt.% LDO content. (Dashed lines indicate the power-law exponents for calculating the surface fractal dimensions.)

Table 1. SAXS parameters* of the composite layers with 40, 60, 80 and 100 wt.% LDO content.

Samples	D_s	Porod constant K_p	a^s (m ² /g)	Surface roughness (nm)	L_c (nm)
100% LDO	2.15	4.86	8.2	1.54	8.83
80% LDO	2.1	3.64	7.4	0.3	6.72
60% LDO	2.05	3.36	7.1	0.2	5.44
40% LDO	2	2.65	5.6	0.2	4.71

* surface fractal dimension (D_s), tail end constant (K_p), specific surface area (a^s), correlation length (L_c).

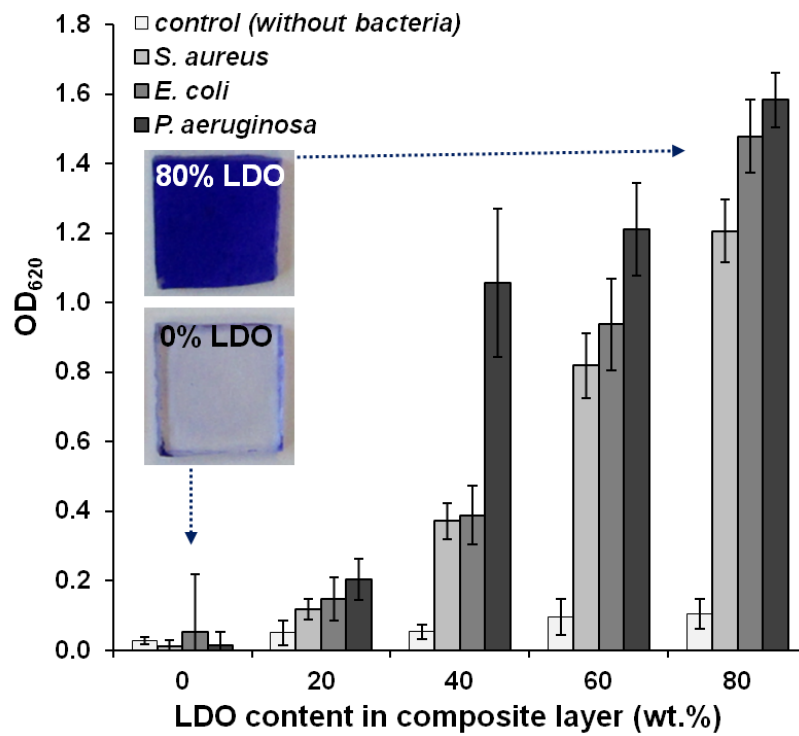


Fig. 6. The microbial adhesion capacity determined with OD₆₂₀ of crystal violet dye released from stained bacterial cells adhering to the surface of the composite layers with different LDO content. The inset shows the crystal violet coloured composite layers (with 0 and 80 wt.% LDO content).

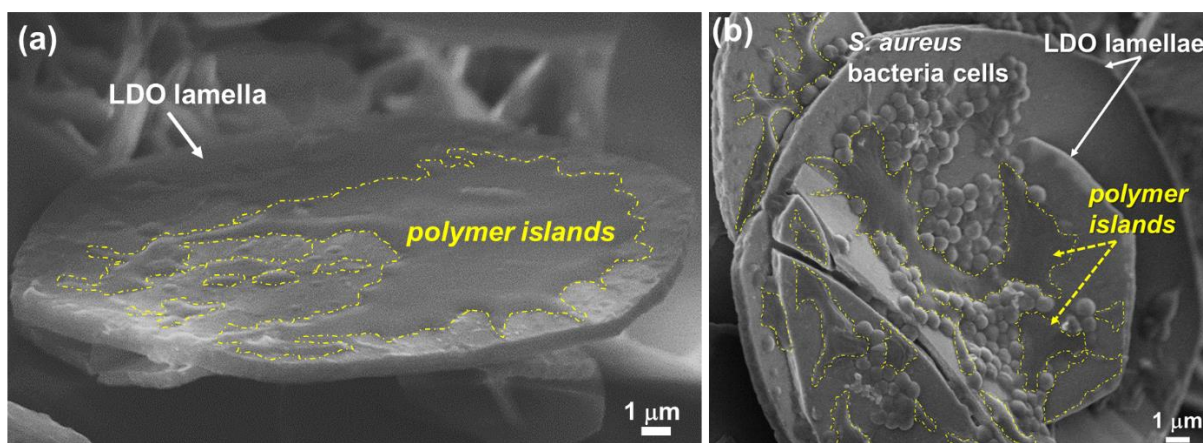


Fig. 7. SEM micrographs of composite layer with a single LDO lamella partially covered by polymer islands (a) and the colony of the adhered *S. aureus* bacteria on the hydrophilic LDO lamellae covered with the unfavorable hydrophobic polymer islands (b).

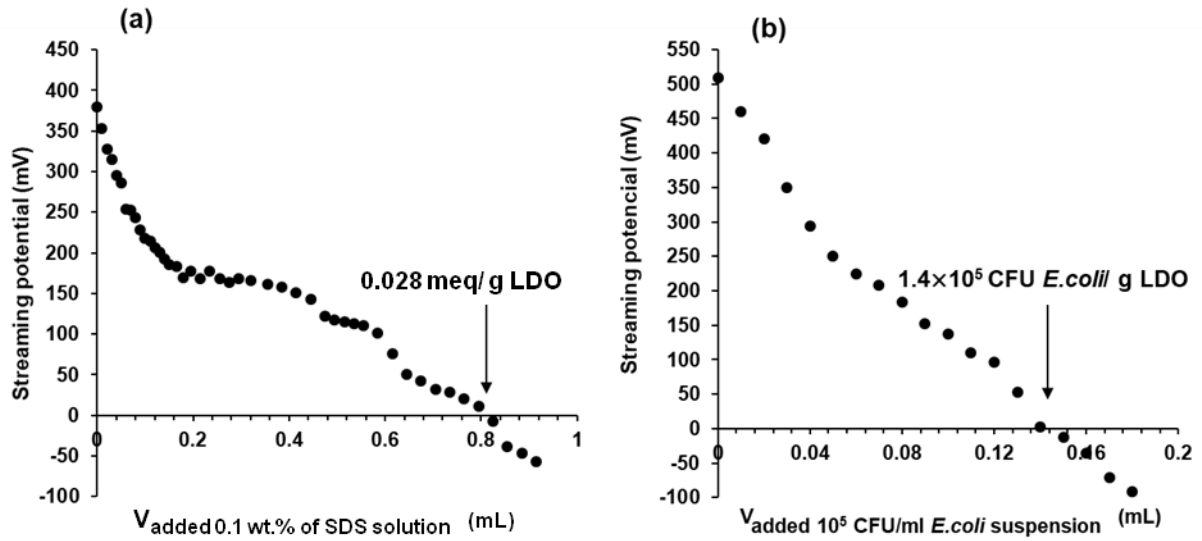


Fig. 8. The charge titration curves of 1 wt.% positively charged LDO suspension (pH = 4.5) with 0.1 wt.% of negatively charged SDS surfactant solution (a) and 10^5 CFU/mL *E. coli* suspension (b).

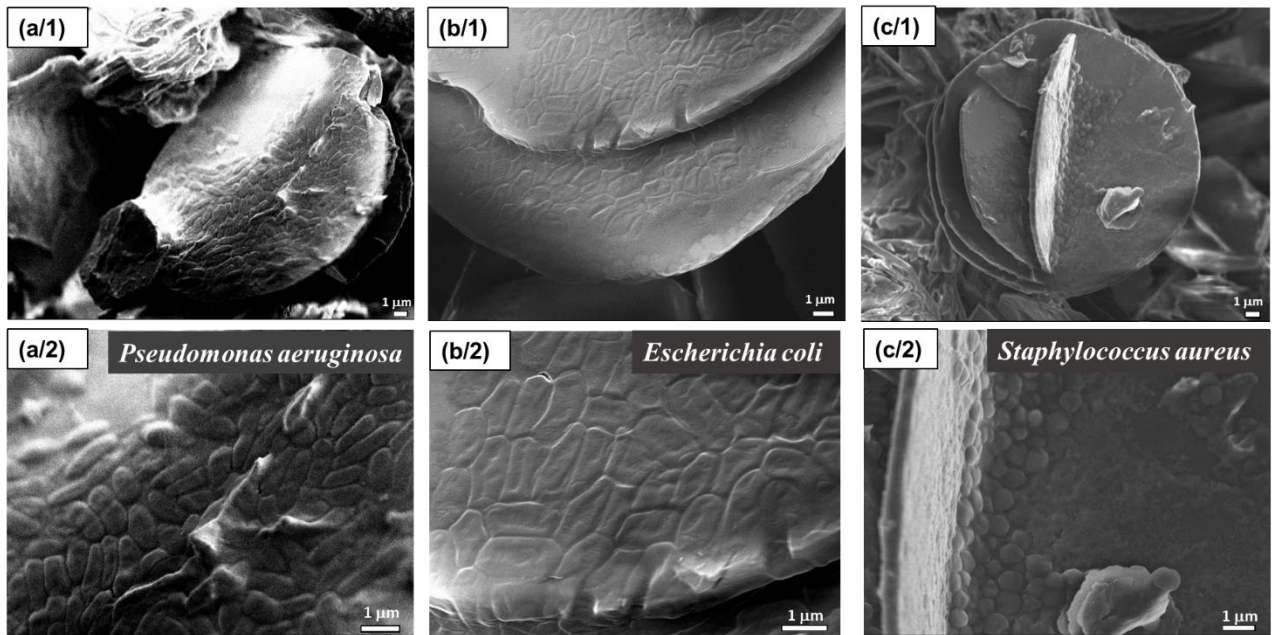


Fig. 9. SEM micrographs of the adhered *P. aeruginosa* (a/1 and a/2), *E. coli* (b/1 and b/2) and *S. aureus* (c/1 and c/2) bacteria on the 80 wt.% LDO containing composite layers after 18 h of bacterial incubation. The majority of bacteria are present on the surface of hydrophilic, high energy LDO particles (see a/2, b/2 and c/2).

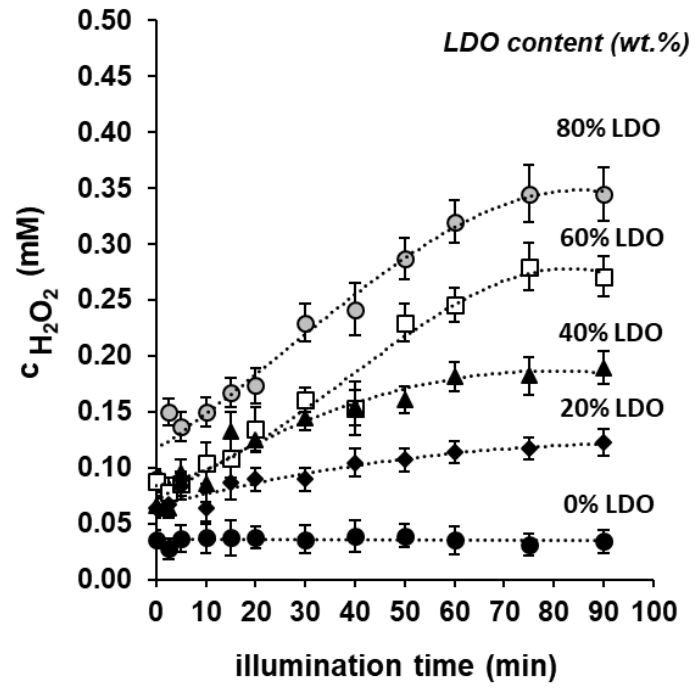


Fig. 10. The equivalent H₂O₂ concentration ($c_{H_2O_2}$) dependence on illumination time for different LDO content is shown.

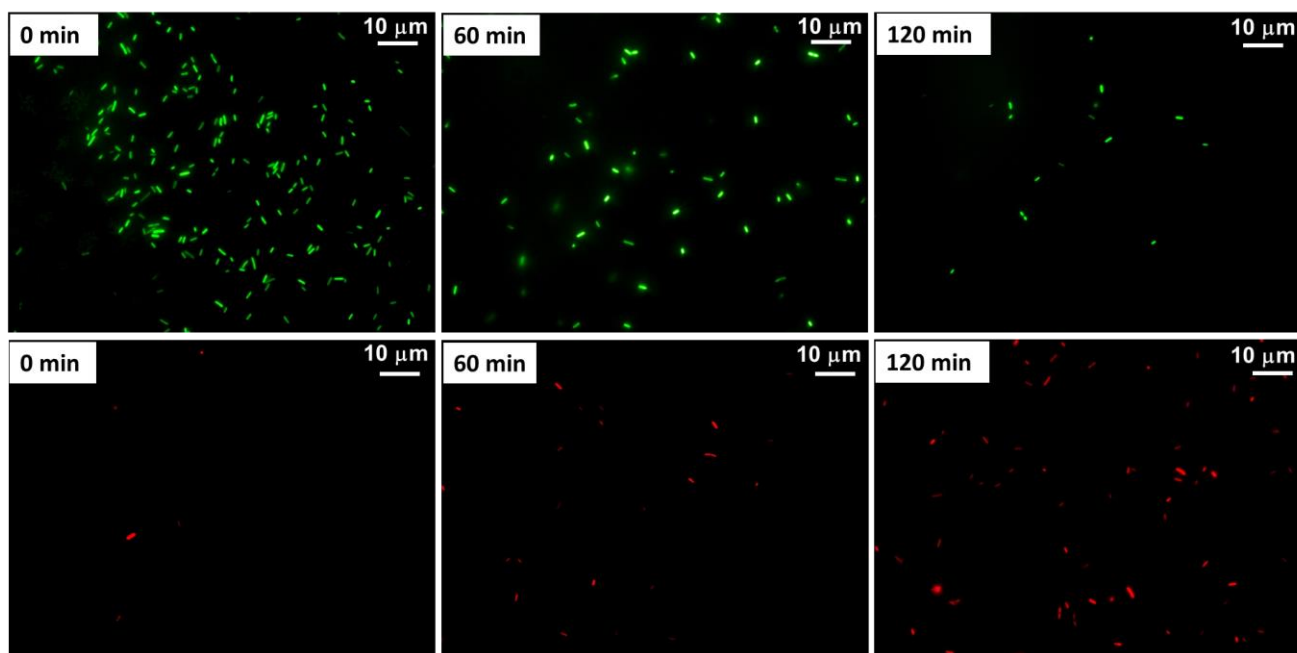


Fig. 11. The viability of *P. aeruginosa* bacterial cells evaluated with fluorescence microscope.

The green parts correspond to live bacteria whereas the red parts corresponds to damaged bacterial cells on the 80 wt.% LDO containing composite layers at the beginning ($t=0$ min) and after 1 and 2 hours of illumination time. The LED-light illumination has wavelength of

$\lambda_{\text{max}}=405$ nm. The inserted scale bars are 10 μm.

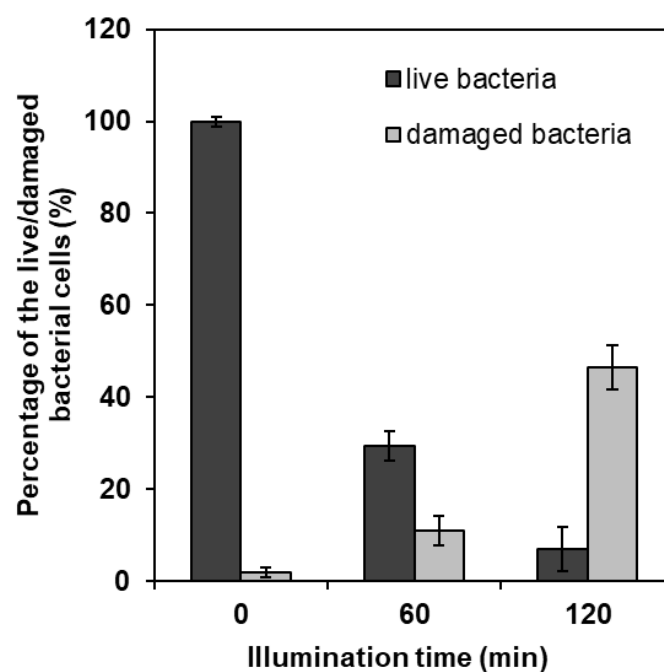
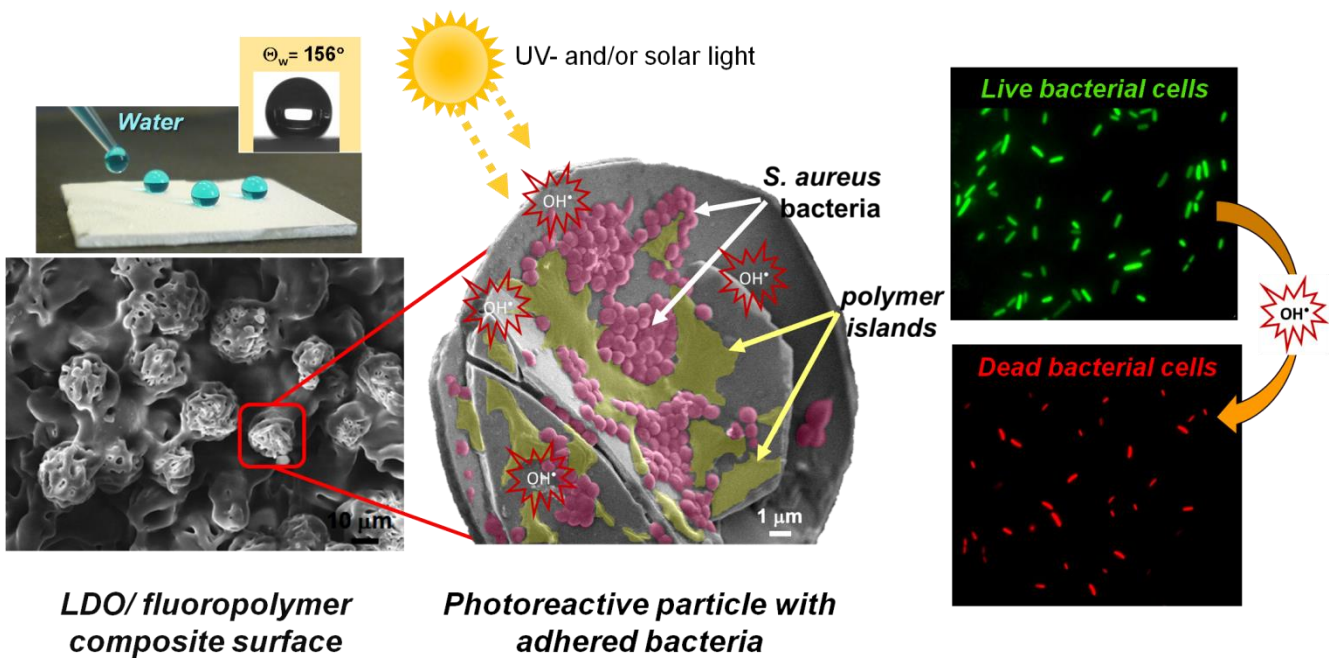


Fig. 12. The percentage of the live and damaged *P. aeruginosa* bacteria adhered on the composite layer as a function of illumination time calculated from the fluorescence microscopy images.

Graphical abstract



Highlights

- Photoreactive composite layers were synthesized with designed wetting properties.
- LDO photocatalysts particles were ensured the adequate surface roughness.
- The adhesion of bacteria was occurred on the photocatalyst (LDO) particles.
- Surface hydrophobicity orientated bacteria were effectively inactivated by light.

Synthesis of self-cleaning and photoreactive spherical layered double oxide/polymer composite thin layers: biofouling and inactivation of bacteria

Ágota Deák^a, László Janovák^{a,*}, Szabolcs Péter Tallósy^b, Karmen Godič-Torkar^c, Anže Abram^{d,e}, Imre Dékány^a, Dániel Sebők^f, Klemen Bohinc^{c,*}

^aUniversity of Szeged, Department of Physical Chemistry and Materials Science, H-6720, Rerrich Béla tér 1, Szeged, Hungary

^bUniversity of Szeged, Institute of Surgical Research, H-6724, Pulz u. 1, Szeged, Hungary

^cUniversity of Ljubljana, Faculty of Health Sciences, Zdravstvena pot 5, 1000 Ljubljana, Slovenia

^dDepartment for Nanostructured Materials, 'Jožef Stefan' Institute, Jamova cesta 39, 1000 Ljubljana, Slovenia

^eJožef Stefan International Postgraduate School, Jamova cesta 39, 1000 Ljubljana, Slovenia

^fDepartment of Applied and Environmental Chemistry, University of Szeged, H-6720, Rerrich Béla tér 1., Szeged, Hungary

*Corresponding author. Tel.: +36 62 544 209; fax: +36 62 544 042.

E-mail address: janovakl@chem.u-szeged.hu (L. Janovák), klemen.bohinc@zf.uni-lj.si (K. Bohinc)

Abstract

Layered double oxide (LDO) photocatalyst microparticles were synthesized with special radial lamellar orientation. We presented that the $25.31 \pm 2.34 \mu\text{m}$ LDO particles with rough surface can be incorporated in fluoropolymer solution and resulted a composite layer with dual

superhydrophobic and photocatalytic properties with high bacterial adhesion and inactivation ability. Next the LDO content in the composite layers were systematically increased (0, 20, 40, 60, 80 and 100 wt.% LDO) which facilitated the surface adhesion of bacteria by electrostatic interactions. The structure of the initial LDO and LDO/fluoropolymer composites was verified by small angle X-ray scattering (SAXS), XRD and SEM measurements. We showed that the surface roughness and hydrophobicity increase with increasing LDO loading. At 80/20 wt.% LDO/fluoropolymer ratio the apparent surface energy was low enough to obtain a superhydrophobic surface ($\theta_w = 156.3^\circ$ and $\gamma_s^{tot} = 2.7 \text{ mJ/m}^2$). The bacterial adhesion extent on LDO/fluoropolymer composite layers increases with increasing LDO content because the adhesion takes place preferentially to LDO lamellae. The reason for this pronounced adhesion of negatively charged and hydrophilic bacteria onto positively charged and hydrophilic LDO surfaces is the electrostatic attraction between oppositely charged surfaces. The bacterial adhesion was detected by scanning electron and fluorescence microscopy and crystal violet staining assay. Finally, the adhered bacteria were inactivated by the LED-light illumination due to photoreactivity of LDO particles containing 12 wt.% of ZnO phase.

Declaration of interests

Ágota Deák^a, László Janovák^a, Szabolcs Péter Tallósy^b, Karmen Godič-Torkar^c, Anže Abram^{d,e},
Dániel Sebők^f, Klemen Bohinc^c, Imre Dékány^{a*}

^aUniversity of Szeged, Department of Physical Chemistry and Materials Science, H-6720, Rerrich Béla tér 1, Szeged, Hungary

^bUniversity of Szeged, Institute of Surgical Research, H-6724, Pulz u. 1, Szeged, Hungary

^cUniversity of Ljubljana, Faculty of Health Sciences, Zdravstvena pot 5, 1000 Ljubljana, Slovenia

^dDepartment for Nanostructured Materials, 'Jožef Stefan' Institute, Jamova cesta 39, 1000 Ljubljana, Slovenia

^eJožef Stefan International Postgraduate School, Jamova cesta 39, 1000 Ljubljana, Slovenia

^fDepartment of Applied and Environmental Chemistry, University of Szeged, H-6720, Rerrich Béla tér 1., Szeged, Hungary

*Corresponding author. Tel.: +36 62 544 210; fax: +36 62 544 042.

E-mail address: i.dekany@chem.u-szeged.hu

☒ The authors declare that they have no known competing financial interests or personal relationships that could have appeared to influence the work reported in this paper.

☐ The authors declare the following financial interests/personal relationships which may be considered as potential competing interests:

--

CrediT authorship contribution statement

Ágota Deák: Methodology, Investigation, original draft

László Janovák: Methodology, Investigation, original draft

Szabolcs Péter Tallósy: Methodology, Investigation, Writing - review & editing

Karmen Godič-Torkarc: Investigatio, Writing - review & editing

Anže Abram: Methodology, Investigation, original draft

Imre Dékány: Conceptualization, Supervision, Funding acquisition, Writing - review & editing

Dániel Sebők: Methodology, Investigation, original draft

Klemen Bohinc: Conceptualization, Writing - review & editing